Electronic Supplementary Information for:

New "X-type" Second-Order Nonlinear Optical (NLO) Dendrimers: Less Chromophore Moieties and High NLO Effects

Runli Tang,[a] Shengmin Zhou,[a] Wendi Xiang, [a] Yujun Xie,[a] Hong Chen,[a] Qian Peng,[b] Gui Yu,[b] Binwen Liu,[c] Huiyi Zeng,[c] Qianqian Li,[a] and Zhen Li [*a]

[a] *Department of Chemistry, Wuhan University, Wuhan 430072, China. E-mail: lizhen@whu.edu.cn; lichemlab@163.com; Fax: (+86) 027 68755363*

[b] *Institute of Chemistry, The Chinese Academy of Sciences, Beijing 100080, China*

[c] *Fujian Institute of Research on the Structure of Matter, the Chinese Academy of Sciences, Fuzhou 350002, China.*

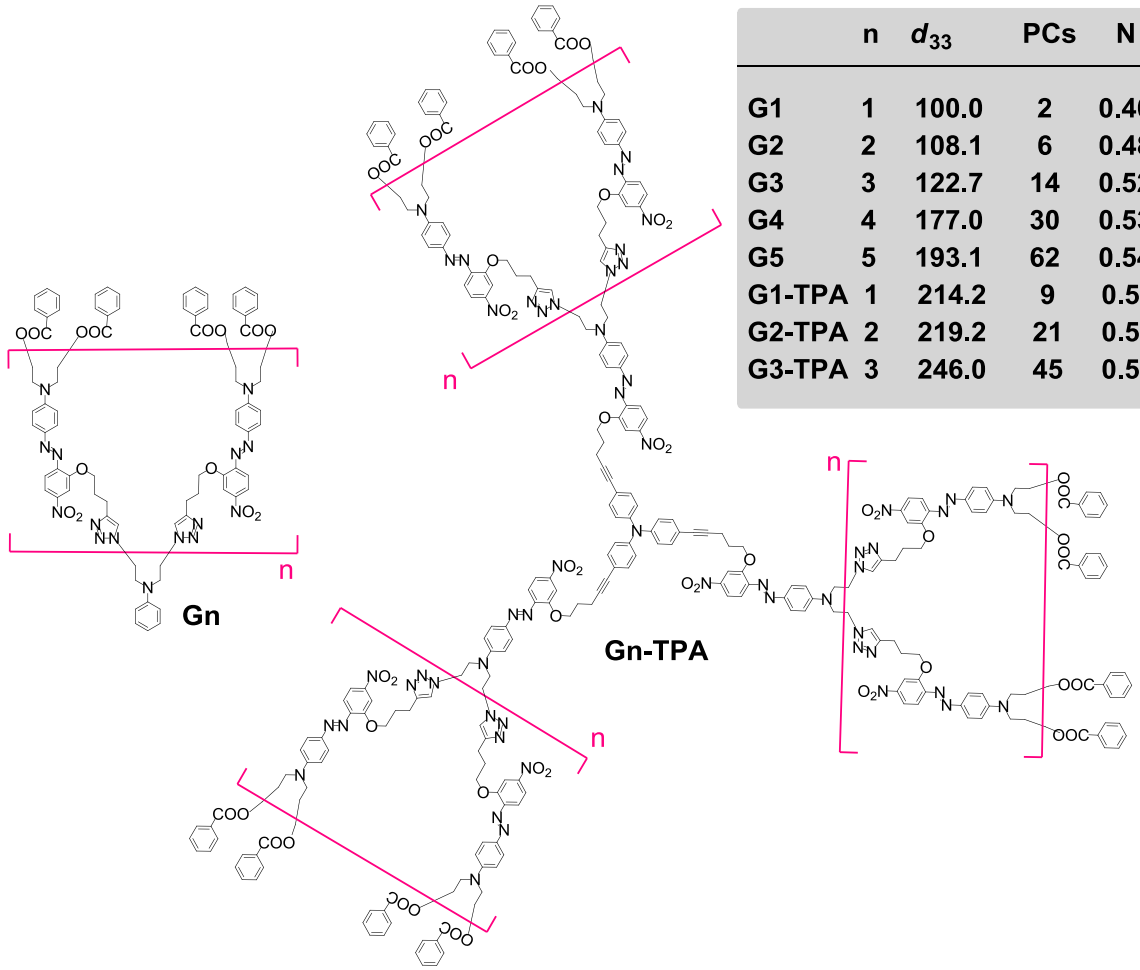

	n	d_{33}	PCs	N
G1	1	100.0	2	0.402
G2	2	108.1	6	0.488
G3	3	122.7	14	0.520
G4	4	177.0	30	0.537
G5	5	193.1	62	0.544
G1-TPA	1	214.2	9	0.502
G2-TPA	2	219.2	21	0.529
G3-TPA	3	246.0	45	0.541

Scheme S1. The structures of dendrimers Gn (n=1-5), global-like dendrimers Gn-TPA and the related parameters: d_{33} (pm/V); PCs (numbers of containing chromophore moiety pieces); N (%, the loading density of the effective chromophore moieties).

Experimental

Materials

Tetrahydrofuran (THF) was dried over Na-K alloy and distilled under an atmosphere of dry nitrogen. N, N-Dimethylform amide (DMF) was dried over CaH_2 and distilled under an atmosphere of dry nitrogen. Compound R1, R2, R3, R4 were prepared according to our previous work[1]. All other reagents were used as received.

Synthesis

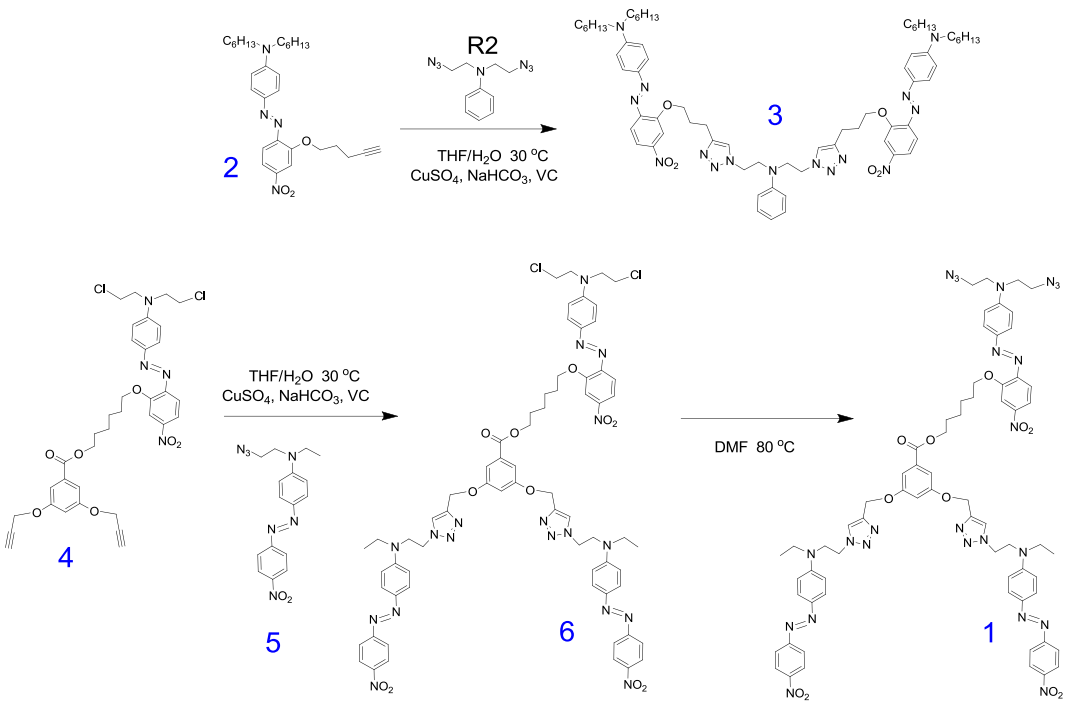

Scheme S3. The synthetic route to other compounds.

Compound **3**: Compound **2** (429.6 mg, 1.0 mmol), compound **R2** (105.1 mg, 0.45 mmol), $CuSO_4$ $5H_2O$ (10 mol %), $NaHCO_3$ (20 mol %), and ascorbic acid (20 mol %) were dissolved in THF (15 mL)/H_2O (3 mL) under nitrogen in a Schlenk flask. The mixture was stirred at 30 ^oC for 2 h, then extracted with chloroform, washed with 1N HCl, 1N NH_4OH and water subsequently. The organic layer was dried over anhydrous magnesium sulfate. After removal of the solvent, the crude product was purified by column chromatography using ethyl acetate/chloroform (1/1) as eluent to afford deep red solid (416.1 mg, 75.3 %). ^1H NMR (300 MHz, $CDCl_3$, 298 K), δ (TMS, ppm): 0.90 (br, s, 12H, -CH_3), 1.33 (br, s, 24H, -CH_2-), 1.61 (br, s, 16H, -CH_2-), 2.23 (br, 4H, -CH_2-), 2.94 (t, J = 6.0 Hz, 4H, -CH_2-), 3.36 (t, J = 7.2 Hz, 8H, -CH_2-), 3.59 (br, 2H, -CH_2-), 4.13 (t, J = 6.0 Hz, 4H, -CH_2-), 4.29 (br, 4H, -CH2), 6.51 (d, J = 7.5 Hz, 2H, -CH2), 6.65 (br, 4H, ArH), 7.16 (br, 3H, ArH), 7.66 (br, 2H, ArH) 7.86-7.78 (br, 8H, ArH). ^{13}C NMR (100 MHz, $CDCl_3$, 298 K), δ (ppm): 13.90, 21.74,

22.54, 26.65, 27.27, 28.40, 31.54, 47.29, 51.21, 51.45, 68.55, 109.28, 111.12, 112.80, 116.56, 117.29, 122.09, 126.29, 129.68, 143.84, 145.74, 146.88, 147.38, 147.77, 151.43, 154.79.

Compound **6**: Compound **4** (65.0 mg, 0.09 mmol), Compound **5** (69.8 mg,0.20 mmol), $CuSO_4$ $5H_2O$ (10 mol %), $NaHCO_3$ (20 mol %), and ascorbic acid (20 mol %) were dissolved in THF (6 mL)/H_2O (1 mL) under nitrogen in a Schlenk flask. The mixture was stirred at 30 ^oC overnight, then extracted with chloroform, washed with 1N HCl, 1N NH_4OH and water subsequently. The organic layer was dried over anhydrous magnesium sulfate. After removal of the solvent, the crude product was purified by column chromatography using ethyl acetate/chloroform (1/1) as eluent to afford deep red solid (100.0 mg, 78.3 %). ^1H NMR (300 MHz, $CDCl_3$, 298 K), δ (TMS, ppm): 1.09 (t, J = 6.6 Hz, 6H, -CH_3), 1.80 (m, 2H, -CH_2-), 1.96 (m, 2H, -CH_2-), 3.22 (m, 4H, -CH_2-), 3.69 (t, J = 6.6 Hz, 4H, -CH_2-), 3.84 (t, J = 6.6 Hz, 4H, -CH_2-), 3.94 (t, J = 5.4 Hz, 4H, -CH_2-), 4.22 (t, 2H, -CH_2-), 4.30 (t, 2H, -CH_2-), 4.60 (t, J = 5.4 Hz, 4H, -CH_2-), 5.17 (br, s, 4H, -CH_2-), 6.70 (d, J = 9.0 Hz, 4H, ArH), 6.77 (d, J = 9.0 Hz, 4H, ArH), 7.23 (d, J = 9.6 Hz, 2H, ArH), 7.54 (br, 2H, ArH), 7.64 (1H, ArH), 7.92-7.84 (m, 7H, ArH), 8.32(d, J = 9.0 Hz, 4H, ArH). ^{13}C NMR (100 MHz, $CDCl_3$, 298 K), δ (ppm): 12.18, 25.92, 28.83, 40.13, 46.70, 48.08, 50.83, 53.88, 62.29, 65.34, 76.95, 78.32, 108.88, 109.79, 111.78, 112.08, 116.66, 117.73, 123.09, 124.15, 124.30, 126.44, 132.55, 143.86, 144.31, 145.08, 147.06, 148.13, 148.90, 149.97, 150.88, 155.62, 156.85, 159.29, 166.77.

Compound **1**: Compound **6** (100.0 mg, 0.07 mmol), NaN_3 (30.0 mg, 0.46 mmol) and DMF (6 mL) were added into a flask, the resultant mixture was allowed to stir at 80 ℃ overnight, and then poured into a lot of water. The precipitate was collected and washed several times with water, dried under vacuum, and purified by column chromatography using ethyl

chloroform/petroleum ether (1/2) as eluent to yield deep red solid (85.0 mg, 85.0%). ^{1}H NMR (300 MHz, $CDCl_3$, 298 K), δ (TMS, ppm): 1.09 (t, J = 7.2 Hz, 6H, -CH_3), 1.80 (m, 2H, -CH_2-), 1.96 (m, 2H, -CH_2-), 3.22 (m, 4H, -CH_2-), 3.57 (m, 4H, -CH_2-), 3.69 (m, 4H, -CH_2-), 3.94 (m, 4H, -CH_2-), 4.22 (2H, -CH_2-), 4.31 (2H, -CH_2-), 4.60 (4H, -CH_2-), 5.17 (4H, -CH_2-), 6.70 (d, J = 9.0 Hz, 4H, ArH), 6.80 (d, J = 9.0 Hz, 4H, ArH), 7.23 (d, J = 9.6 Hz, 2H, ArH), 7.54 (br, 2H, ArH), 7.64 (1H, ArH), 7.92-7.84 (m, 7H, ArH), 8.32(d, J = 8.4 Hz, 4H, ArH). ^{13}C NMR (100 MHz, $CDCl_3$, 298 K), δ (ppm): 12.30, 25.92, 25.95, 28.81, 29.04, 46.09, 47.92, 48.97, 50.64, 50.94, 62.20, 65.41, 69.98, 106.86, 108.91, 109.20, 111.63, 112.04, 116.50, 117.54, 122.94, 124.23, 124.86, 126.35, 132.67, 143.93, 144.28, 145.30, 146.88, 147.69, 148.61, 149.95, 150.48, 155.57, 156.66, 159.29, 166.18.

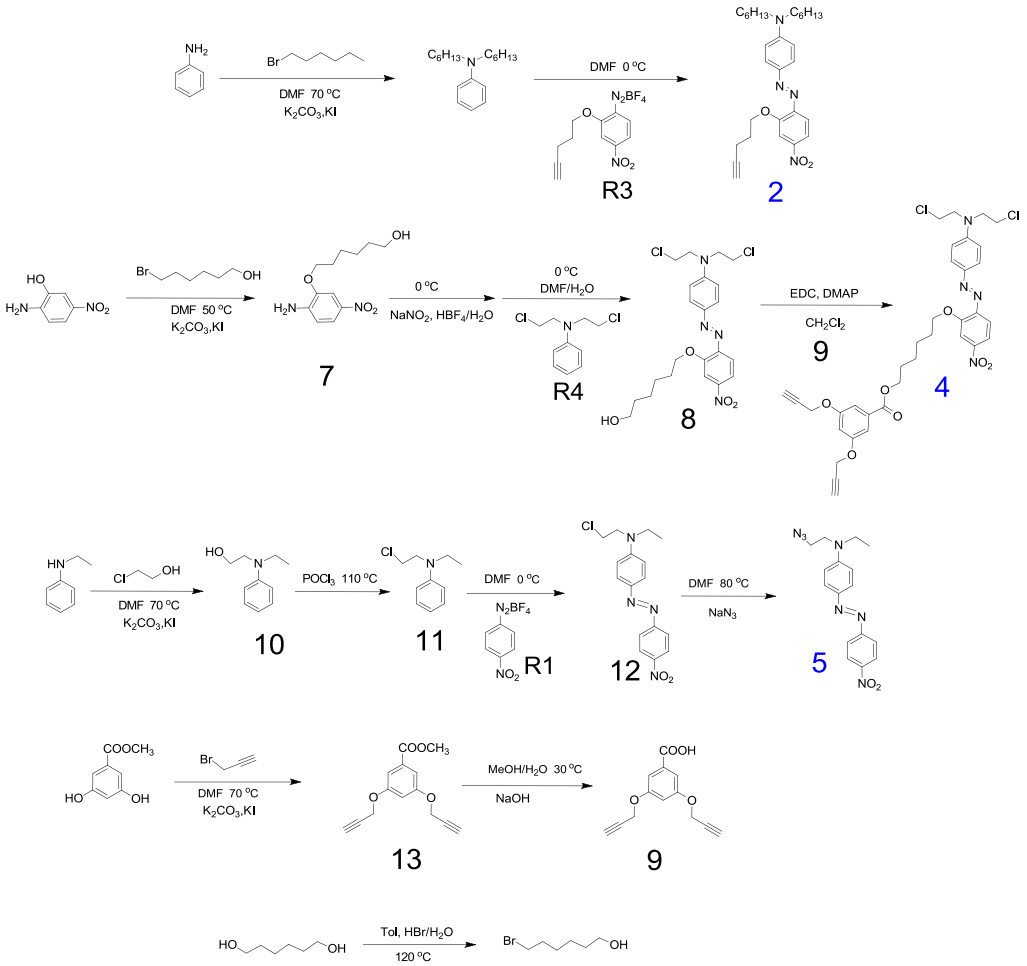

Scheme S4. The synthetic route to other compounds.

***N,N*-Dihexylaniline**: Aniline (2.80 g, 0.03 mol) was dissolved in 30 mL DMF, 1-bromohexane (17.33 g, 0.10 mol), K_2CO_3 (17.43 g, 0.12 mol) and KI (7.42 g, 0.04 mol) were added. After the reaction was stirred for 24 h at 80 ^oC, the mixture was cooled to room temperature, then filtered to remove the solid, and the organic layer was poured into a lot of water. The mixture was extracted with dichloromethane, and washed with water for several times. The organic layer was combined and dried over magnesium sulfate. The crude product was purified by column chromatography on silica gel using dichloromethane/petroleum ether (2/1) as eluent to afford colorless oil. (6.86 g, 87.2 %).

Compound **2**: *N,N*-Dihexylaniline (552.9 mg, 2.0 mmol) and compound **R3** (638.0 mg, 2.0 mmol) were dissolved in 10 mL DMF, stirred for 24 h at 0 ^oC. Then the mixture was poured into a lot of ice water, some sodium bicarbonate was added to adjust pH to ~7.0. Deeply red precipitate was filtered, washed with water. The crude product was purified by column chromatography on silica gel using dichloromethane/petroleum ether (3/1) as eluent. Red powder (826.6 mg, 84.1 %). ^1H NMR (300 MHz, $CDCl_3$, 298 K), δ (TMS, ppm): 0.91 (t, J = 6.3 Hz, 6H, -CH_3), 1.34 (s, 12H, -CH_2-), 1.64 (s, 4H, -CH_2-), 1.99 (t, J = 2.7 Hz, 1H, -C≡H), 2.14 (m, 2H, -CH_2-), 2.51 (m, 2H, -CH_2-), 3.37 (t, J = 7.8 Hz, 4H, -CH_2-), 4.34 (t, J = 6.0 Hz, 2H, -CH_2-), 6.71 (d, J = 8.7 Hz, 2H, ArH), 7.69 (d, J = 9.0 Hz, 1H, ArH), 7.91-7.85 (m, 2H, ArH). ^{13}C NMR (75 MHz, $CDCl_3$, 298 K), δ (ppm): 154.86, 151.43, 147.84, 147.41, 143.88, 126.36, 117.32, 116.74, 111.12, 109.28, 83.27, 77.43, 77.00, 76.58, 69.14, 68.16, 51.30, 31.63, 28.07, 27.32, 26.73, 22.63, 15.15, 14.01.

Compound **7**: 2-Amino-5-nitrophenol (3.08 g, 20.0 mmol), 6-bromohexan-1-ol (3.62 g, 20 mmol), potassium carbonate (4.14 g, 30 mmol) and DMF (40 mL) was added into a flask, and the resultant mixture was stirred at 50 ℃ for the desired time until the complete

consumption of starting material as judged by TLC. Then,100 mL of dichloromethane was added into the reaction mixture, after the salt and DMF was washed out by water, the solvent was removed by evaporation under reduced pressure to afford the crude product, which was further purified by column chromatography on silica gel using chloroform/ethyl acetate (10/1). Yellow solid (4.31 g, 84.8 %). ^{1}H NMR (300 MHz, $CDCl_3$, 298 K), δ (TMS, ppm): 1.26 (m, 2H, -CH_2-), 1.64-1.50 (m, 2H, -CH_2-), 1.87 (m, 2H, -CH_2-), 3.69 (m, 4H, -CH_2-), 4.08 (t, J = 6.6 Hz, 2H, -CH_2-), 4.54 (s, 2H, -NH2), 6.65 (d, J = 8.4 Hz, 1H, ArH), 7.65 (s, 1H, ArH), 7.81 (d , J = 8.4 Hz, 1H, ArH). ^{13}C NMR (100 MHz, $CDCl_3$, 298 K), δ (ppm): 25.70, 26.09, 29.14, 32.78, 63.00, 68.86, 106.76, 111.95, 119.20, 138.85, 143.51, 144.97.

Compound **8**: Compound **7** (2.54 g, 0.01 mol) was dissolved in fluoboric acid (10 mL), the aqueous $NaNO_2$ solution (3 mL-0.90 g) was then added in an ice water bath. After 12 hours, 30 mL of DMF was added into the mixture, and compound **R1** (2.18 g, 0.01 mol) was also added dropwise. After the mixture was stirred at 0 ℃ overnight, 150 mL of dichloromethane into the reaction mixture, then DMF was washed out by water. The solvent was removed by evaporation under reduced pressure to afford the crude product, which was further purified by column chromatography on silica gel using dichloromethane as the eluent. Compound **9** was yielded as red solid (3.95 g, 81.7 %). ^{1}H NMR (300 MHz, $CDCl_3$, 298 K), δ (TMS, ppm): 1.26 (br, 2H, -CH_2-), 1.60-1.49 (m, 4H, -CH_2-), 1.95 ((t, J = 6.9 Hz, 2H, -CH_2-), 3.73-3.66 (m, 6H, -CH_2-), 3.87 (t, J = 6.2 Hz, 4H, -CH_2-), 4.24 ((t, J = 6.9 Hz, 2H, -CH_2-), 6.79 (d, J = 8.7 Hz, 2H, -ArH), 7.67 (d, J = 8.7 Hz, 1H, -ArH), 7.94-7.86 (m, 4H, ArH). ^{13}C NMR (100 MHz, $CDCl_3$, 298 K), δ (ppm): 25.63, 25.98, 29.11, 32.78, 40.39, 53.59, 62.94, 70.04, 109.22, 111.80, 116.46, 117.56, 126.37, 145.39, 146.84, 148.72, 149.65, 155.62.

Compound **4**: Compound **8** (240.0 mg, 0.5 mmol) and **9** (172.6 mg, 0.75 mmol),

1-(3-dimethylaminopropyl)-3-ethylcarbodiimide hydrochloride (EDC) (191.7 mg, 1.0 mmol) 4-dimethylaminopyridine (DMAP) (12.11 mg, 0.1 mmol) were reacted in appropriate anhydrous $CHCl_3$ solution at 30 ℃ overnight under an atmosphere of dry nitrogen. The resultant mixture was washed by citric acid solution and water respectively for several times, the organic layer was dried over magnesium sulfate. The crude product was purified by column chromatography on silica gel using dichloromethane/petroleum ether (1/1) as the eluent. Compound **1** was yielded as red solid (280.0 mg, 80.7 %). ^{1}H NMR (300 MHz, $CDCl_3$, 298 K), *d* (TMS, ppm): 1.61 (br, 2H, -CH_2-), 1.82 (br, 2H, -CH_2-), 1.97(br, 2H, -CH_2-), 2.55 (s, 2H, -CCH), 3.70 (br, 4H, -CH_2-), 3.85 (br, 4H, -CH_2-), 4.24 (br, 2H, -CH_2-), 4.32 (br, 2H, -CH_2-), 4.69 (br, 4H, -CH_2-), 6.79-6.76 (m, 3H, ArH), 7.68-7.65 (m, 4H, ArH), 7.68-7.65 (m, 2H, ArH), 7.93-7.86 (m, 4H, ArH). ^{13}C NMR (100 MHz, $CDCl_3$, 298 K), *d* (ppm): 25.98, 28.79, 29.09, 40.46, 53.66, 56.31, 65.35, 70.10, 76.25, 78.14, 107.29, 109.11, 109.20, 111.84, 116.55, 117.64, 126.40, 132.62, 145.42, 146.90, 148.78, 149.67, 155.62, 158.67, 166.16.

Compound **10**: *N*-ethylaniline (12.10 g, 0.10 mol) were dissolved in 30 mL DMF, 2-chloroethanol (16.10 g, 0.20 mol), K_2CO_3 (13.80 g, 0.10 mol) and KI (3.30 g, 0.02 mol) were added. After stirred for 24 h at 80 ^{o}C, the resultant mixture was cooled to room temperature, filtered to remove the solid, then the organic layer was poured into a lot of water. The mixture was extracted with dichloromethane, and washed with water for several times. The organic layer was dried over magnesium sulfate. The crude product was purified by column chromatography on silica gel using ethyl acetate/petroleum ether (10/1) as eluent to afford colorless oil (7.42 g, 44.8 %).

Compound **11**: Compound **10** (6.93 g, 42.0 mmol) was dissolved in $POCl_3$ (9.69 g, 63.0 mmol) in an ice bath, the mixture was stirred for 2 h at 110 ^{o}C, then cooled to room temperature. Ice water was added into the mixture, then some sodium carbonate solution was used to adjust pH to ~7.0. The

mixture was extracted with chloroform, and the organic layer was combined and dried over magnesium sulfate. The crude product was purified by column chromatography on silica gel using petroleum ether as eluent, to yield colorless oil (6.46 g, 83.7 %).

Compound **12**: Compound **11** (918.4 mg, 5.0 mmol) and compound R**2** (1.184 g, 5 mmol) were dissolved in 8 mL DMF. After stirred for 24 h at 0 ^{o}C, the mixture was poured into a lot of ice water, and some sodium bicarbonate was added to adjust pH to ~7.0. The obtained deep red precipitate was filtered, washed with water, and further purified by column chromatography on silica gel using chloroform/petroleum ether (1/1) as eluent. Compound **7** was yielded as red powder (1.312 g, 78.9 %). ^{1}H NMR (300 MHz, $CDCl_3$, 298 K), δ (TMS, ppm): 1.27 (t, J = 6.9 Hz, 3H, -CH_3), 3.55 (q, J = 6.9 Hz, 2H, -CH_2-), 3.70 (q, J = 7.5 Hz, 2H, -CH_2-), 3.76 (q, J = 7.5 Hz, 2H, -CH_2-), 6.79 (d, J = 9.0 Hz, 2H, ArH), 7.95-7.90 (m,4H, ArH), 8.35(d, J = 8.4 Hz, 2H, ArH). ^{13}C NMR (100 MHz, $CDCl_3$, 298 K), δ (ppm): 12.41, 40.03, 45.82, 52.11, 111.26, 122.59, 124.57, 126.18, 143.85, 147.38, 150.51, 156.51.

Compound **5**: A Schlenk flask was charged with compound **12** (332.7 mg, 1.0 mmol), NaN_3 (130.0 mg, 2.0 mmol) and DMF (10 mL). After stirred at 80 ℃ for 12 h, the resultant mixture was poured into a lot of water. The precipitate was collected, washed with water for several times, dried under vacuum, and purified by column chromatography using ethyl chloroform/petroleum ether (1/1) as eluent. Compound **2** was yielded as red solid (327.0 mg, 96.5 %). ^{1}H NMR (300 MHz, $CDCl_3$, 298 K), δ (TMS, ppm):1.27 (t, J = 6.9 Hz, 3H, -CH_3), 3.63-3.55 (m, 6H, -CH_2-), 6.80 (d, J = 9.6 Hz, 2H, ArH), 7.95-7.90 (m, J = 9.6 Hz, 4H, ArH), 8.35(d, J = 8.4 Hz, 2H, ArH). ^{13}C NMR (100 MHz, $CDCl_3$, 298 K), δ (ppm): 12.40, 46.01, 49.05, 49.66, 111.60, 122.80, 124.82, 126.39, 144.06, 147.57, 150.91, 156.79.

Compound**13**: Methyl 3,5-dihydroxybenzoate (6.81 g, 0.04 mol) was dissolved in acetone, then 3-bromoprop-1-yne (11.8 g, 0.10 mol), K_2CO_3 (13.8 g, 0.10 mol) and KI (2.2 g, 0.02 mol) were added. After stirred for 24 h at 60 ^oC, the mixture was cooled to room temperature, filtered to remove the solid, and then the organic layer was removed to afford yellow solid. The crude product was washed by methanol for several times and recrystallized from acetone/CH_3OH (1/2) to afford pure product (6.44 g, 65.8 %). ^1H NMR (300 MHz, $CDCl_3$, 298 K), δ (TMS, ppm): 2.55 (s, 2H, -C≡H), 3.91 (s, 3H, -CH_3), 4.71 (t, J = 2.4 Hz, 2H, -CH_2-), 6.81 (s, 1H, ArH), 7.29 (s, 2H, ArH).

Compound **9**: Compound **13** (5.85 g, 23.9 mmol) was dissolved in methanol, then NaOH (9.56 g, 23.9 mmol, dissolved in 15mL of H_2O) was added. After stirred for 6 h at 30 ^oC, 20mL of water was added into the mixture, adjusting PH to ~7 using hydrochloric acid, to precipitate the solid. The crude product was washed by water and alcohol for several times, and recrystallized from acetone/CH_3OH (1/1) to afford pure product (4.82 g, 87.3 %). ^1H NMR (300 MHz, $CDCl_3$, 298 K), δ (TMS, ppm): 2.50 (s, 2H, -CCH), 4.84 (t, J = 2.4 Hz, 2H, -CH_2-), 6.85 (s, 1H, ArH), 7.16 (s, 2H, ArH).

6-bromohexan-1-ol: Hexane-1,6-diol (12.90 g, 0.11 mol) was dissolved in 250 mL methylbenzene, 15 mL hydrobromic acid (48 %) was added dropwise. After the reaction was stirred for 24 h at 120 ^oC, the solvent was removed by vacuum distillation to gain the crude product, which was purified by column chromatography on silica gel using chloroform/ethyl acetate (10/1) as eluent to afford colorless oil. (8.87 g, 45.0 %).

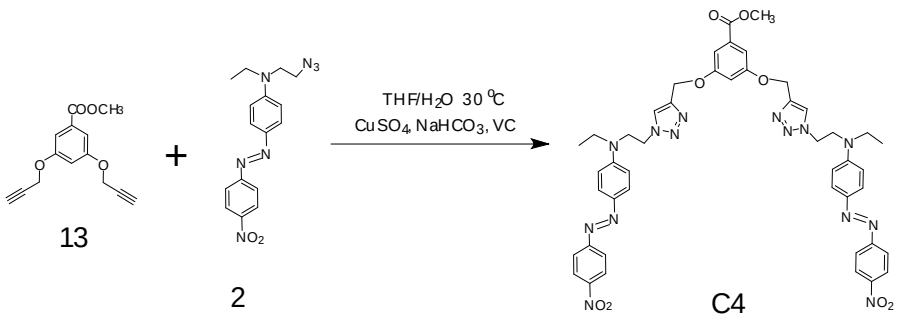

Scheme S5. The synthetic route to other compounds.

Compound **C4**: Compound **2** (51.1 mg, 0.15 mmol), compound **13** (18.3 mg, 0.07 mmol), $CuSO_4$ $5H_2O$ (10 mol %), $NaHCO_3$ (20 mol %), and ascorbic acid (20 mol %) were dissolved in DMF (5 mL)/H_2O (0.5 mL) under nitrogen in a Schlenk flask. The mixture was stirred at 28 ^oC overnight, then extracted with chloroform, washed with 1N HCl, 1N NH_4OH and water subsequently. The organic layer was dried over anhydrous magnesium sulfate. After removal of the solvent, the crude product was purified by column chromatography using chloroform as eluent to afford deep red solid compound **C4** (65.9 mg, 91.5%). ^{1}H NMR (300 MHz, THF, 298 K), δ (ppm): 8.38-8.33 (m, 4H, ArH), 7.98 – 7.90 (m, 8H, ArH), 7.56 (d, J = 5.6 Hz, 2H, ArH), 6.80 (t, J = 2.3 Hz, 1H, ArH), 6.72 (d, J = 9.2 Hz, 4H, ArH), 5.22 (s, 4H, -CH_2-), 4.65 (t, J = 6.2 Hz, 4H, -CH_2-), 3.98 (t, J = 6.2 Hz, 4H, -CH_2-), 3.92 (s, 3H, -CH_3), 3.24 (q, J = 7.1 Hz, 4H, -CH_2-), 1.13 (t, J = 7.1 Hz, 6H, -CH_3). ^{13}C NMR (75 MHz, $CDCl_3$, 298 K), δ (ppm): 166.44, 159.08, 156.50, 150.21, 147.59, 144.17, 143.81, 132.19, 126.27, 124.67, 123.88, 122.75, 111.46, 108.68, 107.03, 77.43, 77.20, 77.00, 76.58, 62.01, 52.38, 50.44, 47.73, 45.90, 12.09. (EA) (%, found/Calcd): C, 59.47/59.86; H, 5.43/5.02; N, 21.01/21.25.

NLO Measurement

Nonlinear optical coefficients

The polarization $p^{2\omega}$ cos 2ωι in a nonlinear medium by an optical electric field E^{ω} sin ωι was stated as:[2]

$$p_i^{2\omega} = \chi_{ijk}^{2\omega} E_j^{\omega} E_k^{\omega} \tag{1}$$

$\chi_{ijk}^{2\omega}$ is a (3×3×3) third tensor, considering a particular physical situation, the two symmetric suffixes *j* and *k* are replaced by a single suffix m, the relation is:

m =	1	2	3	4	5	6
jk =	xx	yy	zz	yz	zx	xy

(2)

It also can be described as:

$$\chi_{ijk}^{2\omega}(-2\omega_1;\omega_1\omega_1) = d_{ijk}(-2\omega_1;\omega_1\omega_1) \tag{3}$$

So the polarization *p* can be described as:

$$\begin{bmatrix} p_1 \\ p_2 \\ p_3 \end{bmatrix} = \varepsilon_0 \begin{bmatrix} d_{11} & d_{12} & d_{13} & d_{14} & d_{15} & d_{16} \\ d_{21} & d_{22} & d_{23} & d_{24} & d_{25} & d_{26} \\ d_{31} & d_{32} & d_{33} & d_{34} & d_{35} & d_{36} \end{bmatrix} \begin{bmatrix} E_1^2 \\ E_2^2 \\ E_3^2 \\ 2E_1\ E_3 \\ 2E_1\ E_2 \\ 2E_2\ E_3 \end{bmatrix} \tag{4}$$

For the sample lattice such as transparent crystals, if the absorption of fundamental beam or the second harmonic beam is negligible, the 18 independent coefficients can be condensed to 10: [3] $d_{12}= d_{26}$, $d_{13}= d_{35}$, $d_{14}= d_{25}= d_{36}$, $d_{15}= d_{31}$, $d_{16}= d_{21}$, $d_{23}= d_{34}$, $d_{24}= d_{32}$.

Therefore, in the most general cases, there are 10 independent coefficients as follows:

$$\begin{bmatrix} d_{11} & d_{12} & d_{13} & d_{14} & d_{15} & d_{16} \\ d_{16} & d_{22} & d_{23} & d_{24} & d_{14} & d_{12} \\ d_{15} & d_{24} & d_{33} & d_{23} & d_{13} & d_{14} \end{bmatrix} \tag{5}$$

According to the Kleiman symmetry above, the SiO_2 -quartz structure with D_3 symmetry a typical example of the polar structure, has only one independent coefficient. In this paper, Y-cut quartz serves as the reference, which dominates the d_{33} value of the samples.

It deserves to be noted that, the absorptions of the thin films of **C1**, **C2** and **C3** have some overlaps with the second harmonic beam (532 nm), the Kleinman's symmetry is not fully satisfied to some extent. However, to use the 1064 nm laser, a common fundamental beam to measure the SHG signals, is still a convenient and effective method. With the purpose of reducing the influence of UV absorption, another test under 1950 nm fundamental beam was also carried out.

Within the two-level model of molecular nonlinearities, the resonantly enhanced hyperpolarizability can be expressed as:[4]

$$\beta(\omega) = \mathrm{R}(\omega) \times \beta_0 \tag{6}$$

Where β_0 is the nonresonant value and the resonance enhancement factor is:

$$\mathrm{R}(\omega) = \frac{{\omega_0}^4}{({\omega_0}^2 - \omega^2) \times ({\omega_0}^2 - 4\omega^2)}, \quad \omega_0 = \frac{2\pi c}{\lambda_{\max}} \tag{7}$$

Where λ_{max} is the wavelength at which the maximum of the principal absorption band occurs, and ω corresponds to the wavelength of the laser.

$d_{33(\infty)}$ was calculated using this approximate model:

$$d_\infty = d_{33} \times \left[1 - \left(\frac{\lambda_{\max}}{\lambda}\right)^2\right] \times \left[1 - 4\left(\frac{\lambda_{\max}}{\lambda}\right)^2\right] \tag{8}$$

Where λ_{max} was the wavelength of maximum absorption, λ was the wavelength of the fundamental laser.

Preparation of thin films

The samples were dissolved in THF (concentration ~3 wt %), and the solutions were filtered through syringe filters. The thin films were spin-coated onto indium-tin-oxide (ITO)-coated glass substrates, which were subjected to ultrasonication in different solvent systems including 2% soap in water, acetone, deionized water, DMF, THF. Each step was

carried out for 20 min. Residual solvent of the thin films was removed by heating the films in a vacuum oven at 45 ^{o}C.

Measurement condition

The second-order optical nonlinearity of the materials was determined by in-situ second harmonic generation (SHG) experiment by using a closed temperature-controlled oven with optical windows and three needle electrodes. The films were kept at 45^{o} to the incident beam and poled inside the oven, and the SHG intensity was monitored simultaneously. Poling conditions were as follows: temperature, different for each polymer (Table 3); voltage, 7.0 kV at the needle point; gap distance, 0.8 cm. The SHG measurements were carried out with a Nd:YAG laser operating at a 10 Hz repetition rate and an 8 ns pulse width at 1064 nm.

The NLO efficiencies were also investigated using 1950 nm laser radiation. The doubled frequency signals (975 nm) were detected by an Andor's DU420A-BR-DD CCD after the mixed signals passed through the monochromator.

Stability and error analysis

The d_{33} value of each dendrimer was measured by averaging the testing values of repeated measurements, including that of the same film and different films of the specific molecule (eq. 9). Film thickness and intensity ratio are two parameters to calculate the d_{33} value of the sample. Where the intensity ratio is I_{film} (signal intensity of thin film) divided by I_{quartz} (signal intensity of quartz).

$$\text{Average } d_{33} \begin{cases} d_{33} \text{ of film1} \begin{cases} \text{Intensity Raio} = I_{film} / I_{quartz} \\ \text{Film thickness} \end{cases} \\ d_{33} \text{ of film2} \begin{cases} \text{Intensity Raio} = I_{film} / I_{quartz} \\ \text{Film thickness} \end{cases} \\ d_{33} \text{ of film3} \begin{cases} \text{Intensity Raio} = I_{film} / I_{quartz} \\ \text{Film thickness} \end{cases} \end{cases} \tag{9}$$

The error of film thickness is ±3.1 nm, the error of SHG measurement is 10 %, [5] the error of d_{33} value is the sum of the previous two.

The value of SHG signal intensity was automatically generated by a software, averaging the value of sampling signals. Figure S1 showed the values of SHG signals of quartz and sample, and the intensity ratio. Under the laser with a certain power, the quartz was firstly measured, then the sample. It was measured under laser with four different intensities, from left to right: as the laser strength increased, the SHG intensity of quartz and sample increased, while the intensity ratio of sample/quartz remained the same. Under the laser with the same strength, the SHG signal of the sample keep stable, thus, errors could be reduced by averaging the signal values.

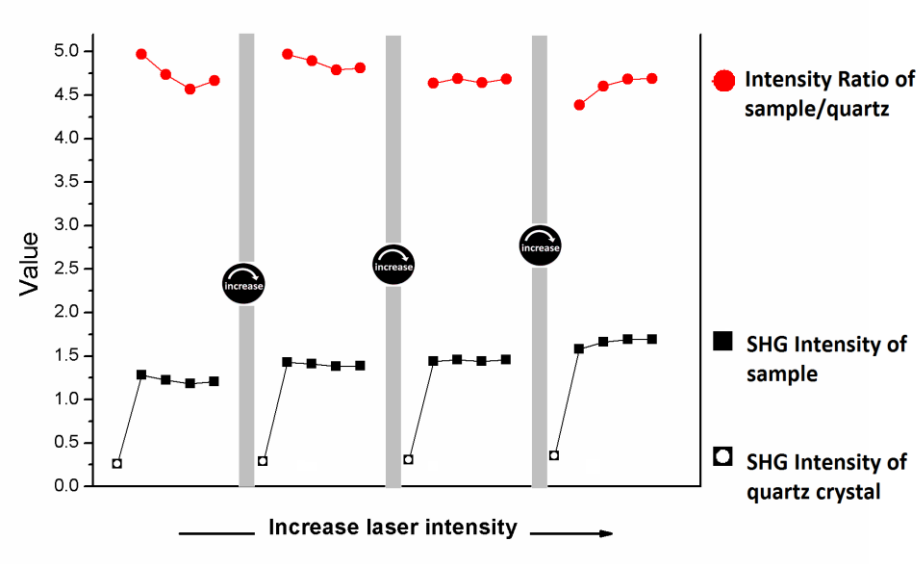

Fig.S1. The value of SHG signal and the intensity ratio under the laser of four different intensities (compound C2 as the sample).

Calculation

Methods

The ground-state geometries of the fragments Frag1-Frag3 were firstly optimized by using semi-empirical PM6 method, and then further optimized by employing DFT with B3LYP functional[6]

and 6-311G (d,p) basis set in vacuum. The vibrational frequencies were calculated at the ground-state equilibrium geometries at the same DFT level. In comparison with the experiments, the vibrational frequency scaling factor of 0.967 [7] was used to offset the systematic errors caused by basis set incompleteness, neglecting the electron correlating and vibrational anharmonicity.

In order to obtain the configurations of the whole dendrimer molecule, the molecular mechanics (MM) simulations were firstly carried out by using the Discover module from Materials studio (MS) software package[8]. Herein, the polymer consistent force field (PCFF), was used to optimize structures, and the minimization method was Smart Minimizer. Based on the simulated structures, the further optimizations were performed for **C1** (186 atoms), **C2** (323 atoms), and **G1** (196 atoms) at B3LYP/6-31G (d) level, and for **C3** (595 atoms) and **G2** (453 atoms) at B3LYP/STO-3G level. The calculated structures and the molecular orbitals (HOMO and LUMO) were plotted in Figure S42-S46 (ESI†). Although MM simulation and the quantum chemical calculation gave slightly different results in some bond lengths and angles, leading to a little difference of the orientation of chromophore moieties, they offered similar molecular configuration orders. All of the quantum chemical calculations were performed in Gaussian 09 program package.[9]

Results and discussion

We performed a molecular mechanics simulation for **C1**, **C2**, **C3**, and also for **G1**, **G2** for comparison (the calculation method and detailed information were presented in ESI†). Fig. **S2** showed the conformation of each compound from three viewpoints: Front-view, Top-view, and Side-view. The Front-view was based on the xy plane (colored as gray), which was set on the center chromophore (marked as ball and stick style), the Top- and Side-view were captured, rotating front-plane on its x- and y-axis, respectively. For comparison, **G1** and **G2** were calculated under the same conditions. As easily seen, all the molecules had multi-azimuth 3D structures, **C1** and **G1** had

similar conformations: approximately planar, and all the chromophore moieties were exposed to the interface, leading to the strong interactions of the electrical dipole moments. This was supposed to be the main reason for their low NLO effects. In contrast, other molecules exhibited 3D-extended conformations. Especially, the conformation of **C3** was almost spherical, the best conformation to achieve large NLO effect. Meanwhile, the orientation of the chromophore moieties on the molecular scale could be observed in the figure clearly. Actually, the original orientation of the chromophore moieties was very important for the final NLO effect, since it badly affected the poling procedure directly. For **C1** and **G1**, the dipolemoments counteracted with each other to a certain extent, thus, perhaps, the orientation provided little contribution to their macroscopic NLO effect as they were nearly small planar molecules. For **C2**, the covalent bonds constrained the motion of the five chromophore moieties ordered, and partially due to the steric hindrance, the dipolemoments did not counteract with each other too much, but were remained to an ordered orientation to some extent. This may be the reason that **C2** had a much larger NLO effect. **C3** was the most chromophore-rich and spherical molecule. Although the outside chromophore moieties were not arranged orderly, the "**C2**" part (five chromophore moieties) of **C3** was ordered and well protected. Also, there was some room for the chromophore moieties orienting to be orderly aligned upon poling, as a result of its spherical conformation. Thus, **C3** reached a high SHG coefficient.

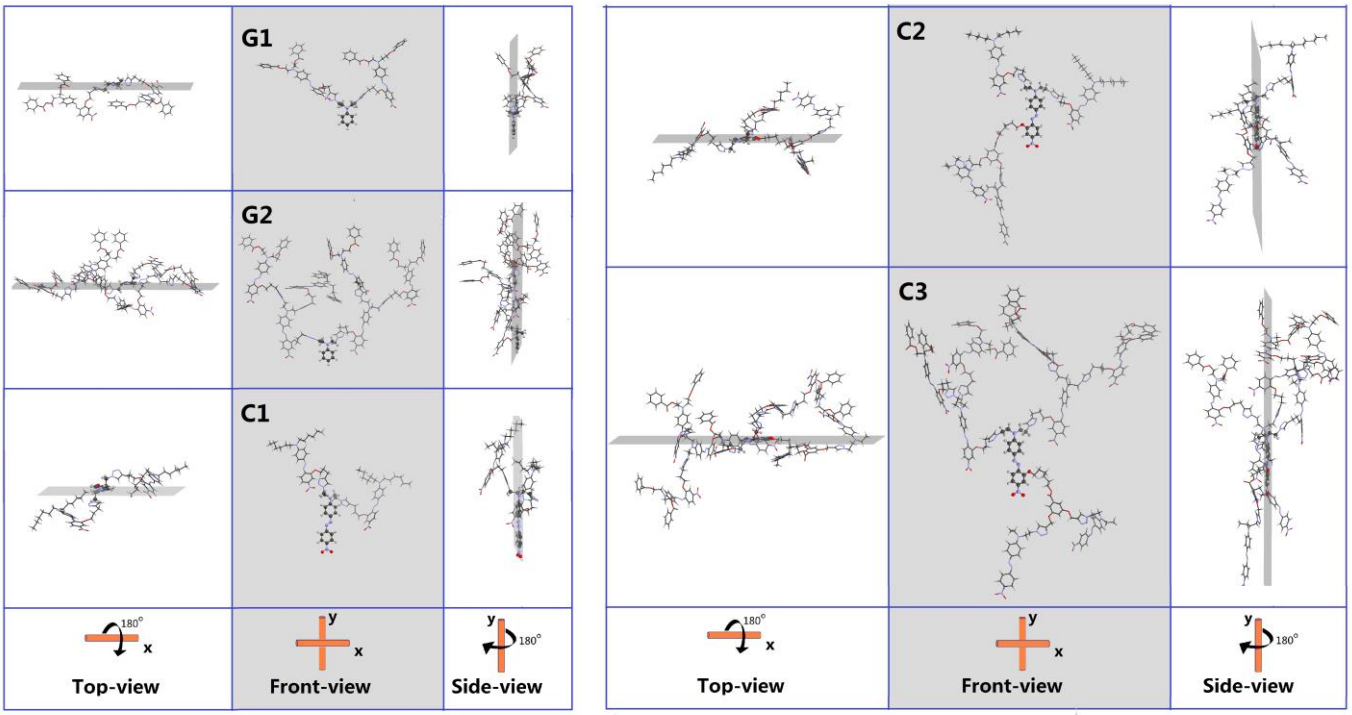

Fig. S2 Molecular conformations calculated by MD simulation (Front-view based on the xy-plane, Top-view and Side-view were rotated xy-plane on its x-axis and y-axis respectively).

References

1 (a) Z. Li, Z. Li, C. Di, Z. Zhu, Q. Li, Q. Zeng, *Macromolecules*, 2006, **39**, 6951; (b) Z. Li, Q. Zeng, Z. Li, S. Dong, Z. Zhu, Q. Li, *Macromolecules*, 2006, **39**, 8544; (c) Q. Li, Z. Li, Zeng F, Gong W, Z. Li, Z. Zhu, *J. Phys. Chem. B.*, 2007, **111**, 508; (d) Q. Li, Z. Li, C. Ye, J. Qin. *J. Phys. Chem. B.*, 2007, **112**, 4928; (e) Z. Li, S. Dong, G. Yu, Z. Li, Y. Liu, C. Ye, *Polymer*, 2007, **48**, 5520; (f) Z. Li, P. Li, S. Dong, Z. Zhu, Q. Li, Q. Zeng, Z. Li, *Polymer*, 2007, **48**, 3650; (g) Z. Zhu, Q. Li, Q. Zeng, Z. Li, Z. Li, J. Qin, *Dyes. Pigm.*, 2008, **78**, 199; (h) Z. Li, G. Yu, S. Dong, W. Wu, Y. Liu, C. Ye, *Polymer*, 2009, **50**, 2806; (i) Z. Li, W. Wu, P. Hu, X. Wu, G. Yu, Y. Liu, Z. Li, *Dyes. Pigm.*, 2009, **81**, 264; (j) Z. Li, W. Wu, C. Ye, J. Qin, Z. Li. *J. Phys. Chem. B.*, 2009, **113**, 14943; (k) Z. Li, Q. Zeng, G. Yu, Z. Li, C. Ye, Y. Liu, Z. Li, *Macromol. Rapid. Commun.*, 2008, **29**. 136; (l) Q. Zeng, Z. Li, Z. Li, C. Ye, J. Qin, B. Z. Tang, *Macromolecules*, 2007, **40**, 5634.

2 Franken P. A., Ward J. F., *Rev. Mod. Phys.*, 1963, **35**, 23-29.

3 Kleiman D. A., *Phys. Rev.*, 1962, **126**, 1977.

4 Martti Kauranen, Thierry Verbiest, Carlo Boutton, M. N.Teerenstra, Koen Clays, A. J. Schouten, R. J. M.Nolte, Andre Persoons., *Science.*, 1995, **270**, 966.

5 W. Wu, C. Wang, Q. Li, C. Ye, J. Qin, Z. Li, *Sci. Rep.*, 2014, **4** , 6101.

6 (a) A. D. Becke, *J. Chem. Phys*., 1993, **98**, 5648; (b) C. Lee, W, Yang, R. G. Parr, *Phys. Rev. B.*, 1988, **37**, 785.

7 M. P. Andersson and P. Uvdal, *J. Phys. Chem. A.*, 2005, **109**, 2937.

8 (a) H. Yang, F. Fang, C. Zhao, D. Li, J. Li, J. Sun, Q. Du, H. Zhu, *Med. Chem. Commun.*, 2014, **5**, 219; (b) W. Tian, Y. Ma, *Chem. Soc. Rev.*, 2013, **42**, 705.

9 Gaussian 09, Revision A.02, M. J. Frisch, G. W. Trucks, H. B. Schlegel, G. E. Scuseria, M. A. Robb, J. R. Cheeseman, G. Scalmani, V. Barone, B. Mennucci, G. A. Petersson, H. Nakatsuji, M. Caricato, X. Li, H. P. Hratchian, A. F. Izmaylov, J. Bloino, G. Zheng, J. L. Sonnenberg, M. Hada, M. Ehara, K. Toyota, R. Fukuda, J. Hasegawa, M. Ishida, T. Nakajima, Y. Honda, O. Kitao, H. Nakai, T. Vreven, J. A. Montgomery, Jr., J. E. Peralta, F. Ogliaro, M. Bearpark, J. J. Heyd, E. Brothers, K. N. Kudin, V. N. Staroverov, R. Kobayashi, J. Normand, K. Raghavachari, A. Rendell, J. C. Burant, S. S. Iyengar, J. Tomasi, M. Cossi, N. Rega, J. M. Millam, M. Klene, J. E. Knox, J. B. Cross, V. Bakken, C. Adamo, J. Jaramillo, R. Gomperts, R. E. Stratmann, O. Yazyev, A. J. Austin, R. Cammi, C. Pomelli, J. W. Ochterski, R. L. Martin, K. Morokuma, V. G. Zakrzewski, G. A. Voth, P. Salvador, J. J. Dannenberg, S. Dapprich, A. D. Daniels, O. Farkas, J. B. Foresman, J. V. Ortiz, J. Cioslowski, and D. J. Fox, Gaussian, Inc., Wallingford CT, 2009.

The ^{1}H NMR and ^{13}C NMR spectra of related compounds:

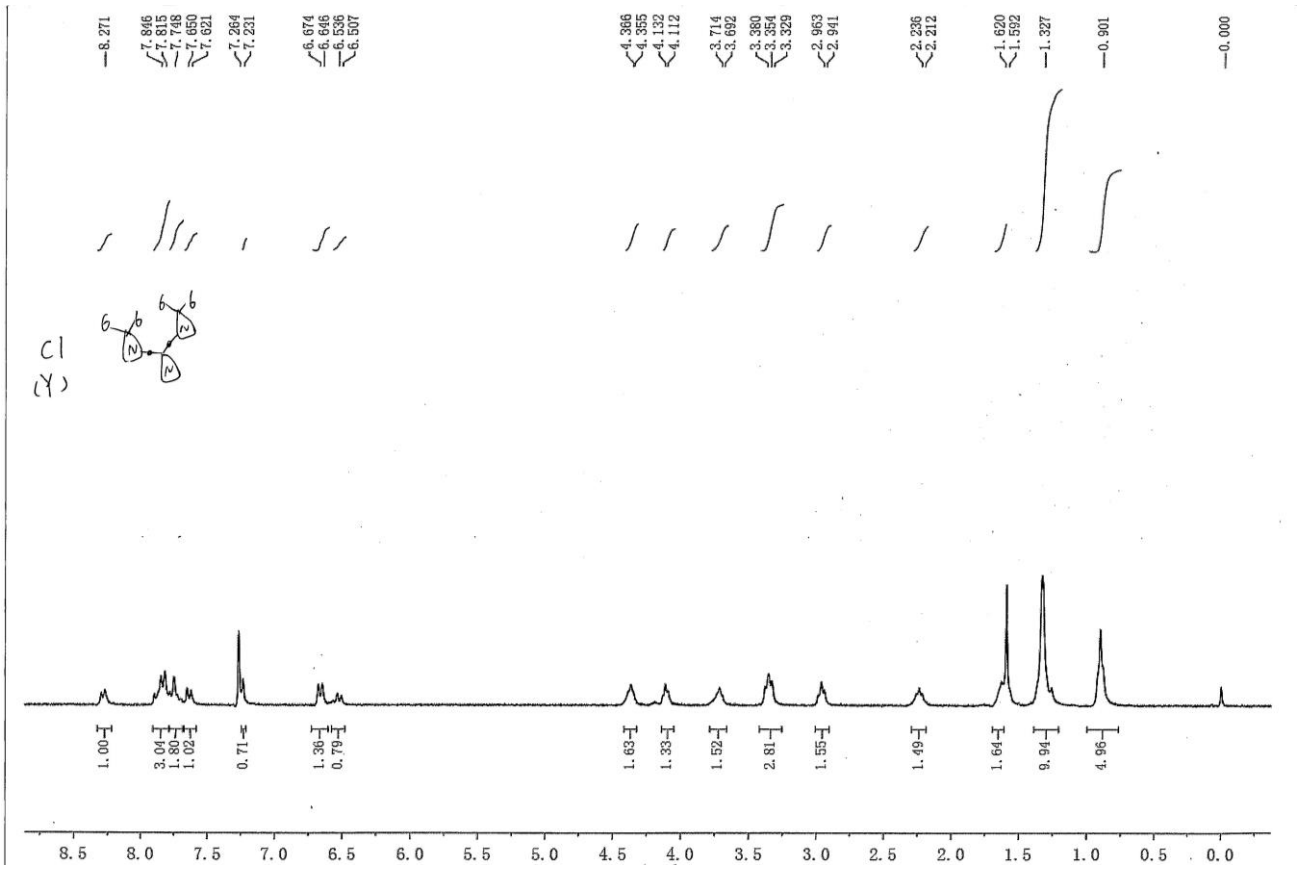

Fig.S3. ^{1}H NMR spectrum of compound **C1** in chloroform-*d*.

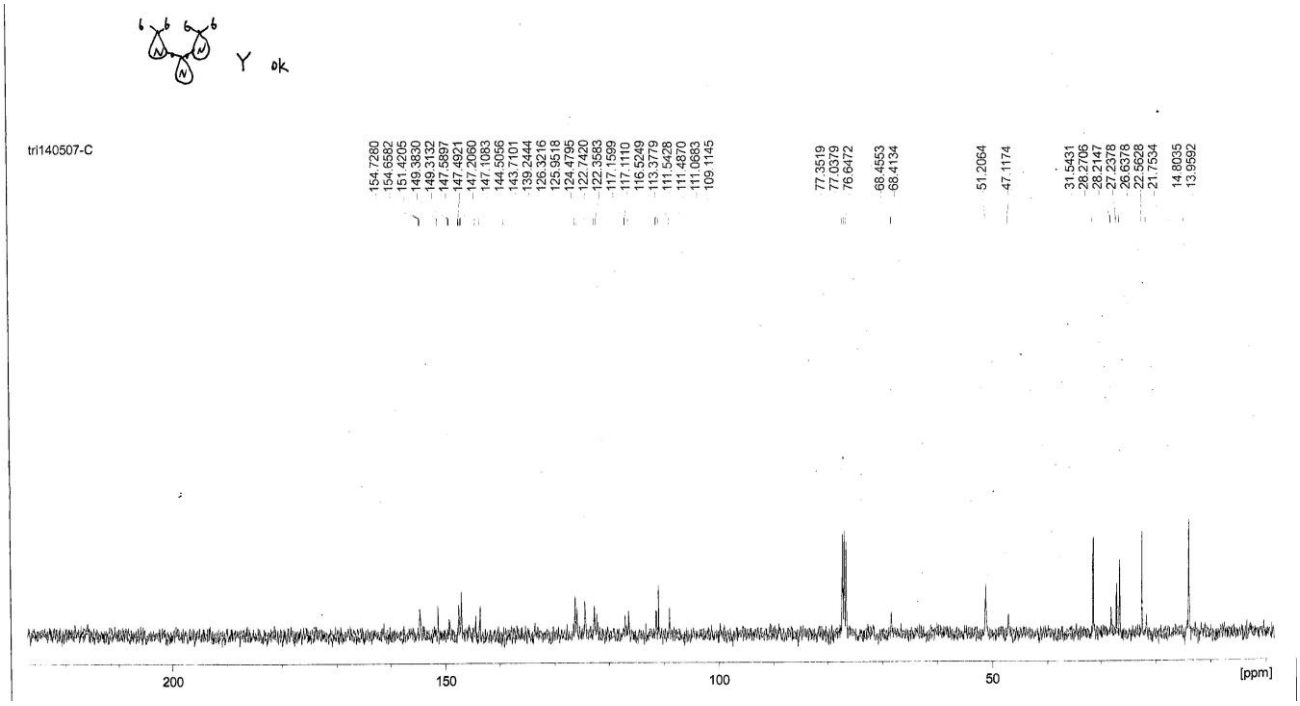

Fig.S4. ^{13}C NMR spectrum of compound **C1** in chloroform-*d*.

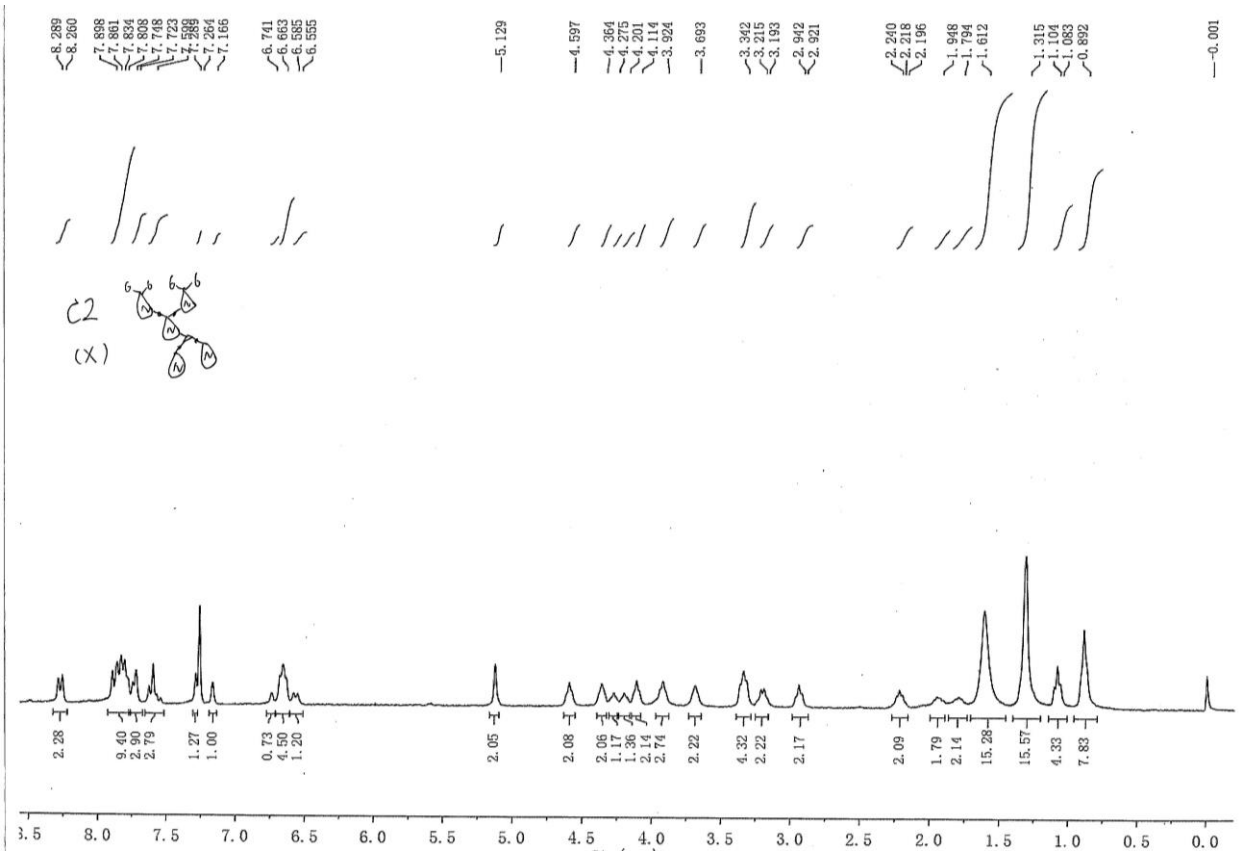

Fig.S5. ^{1}H NMR spectrum of compound **C2** in chloroform-*d*.

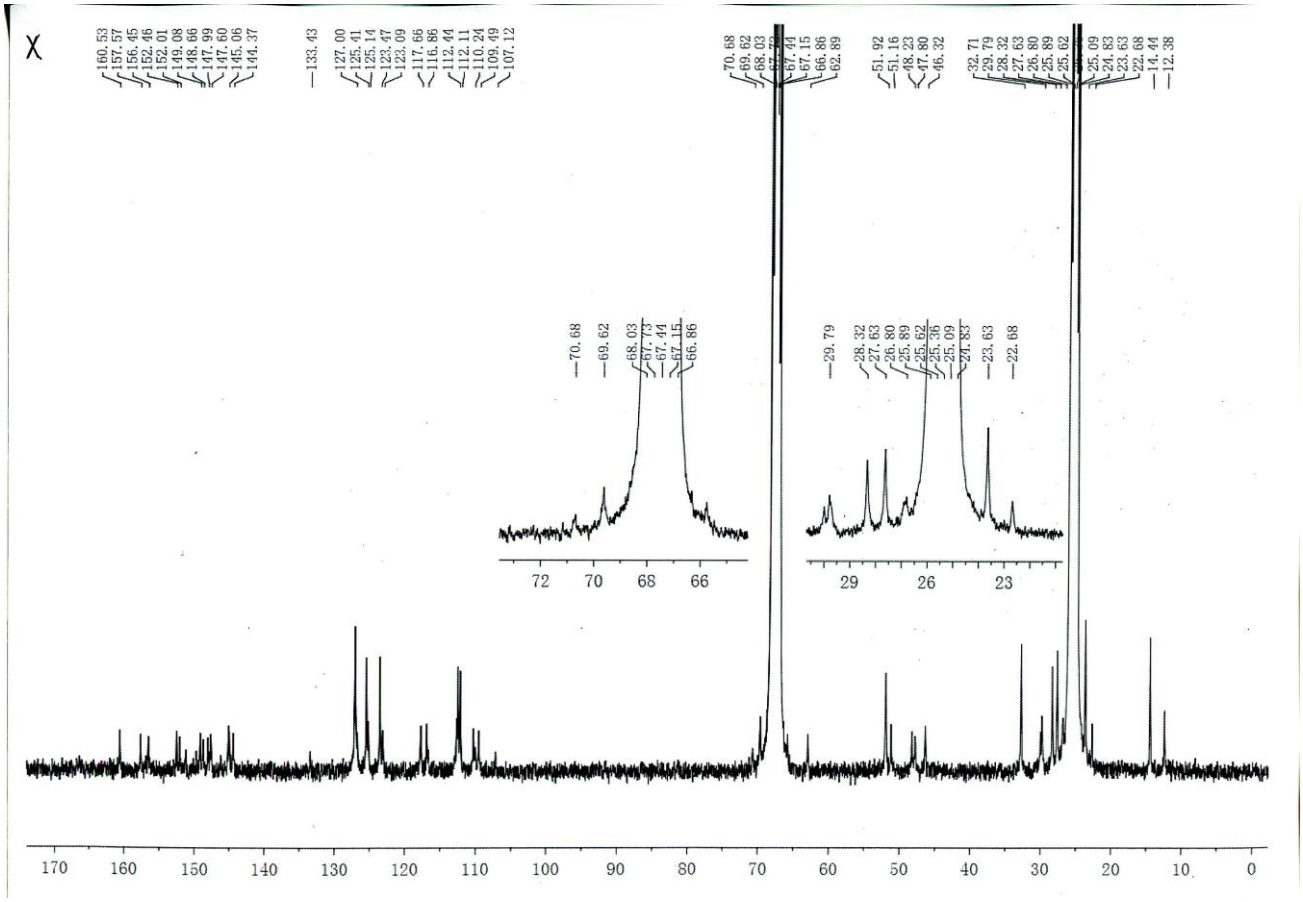

Fig.S6. ^{13}C NMR spectrum of compound **C2** in THF-d_8.

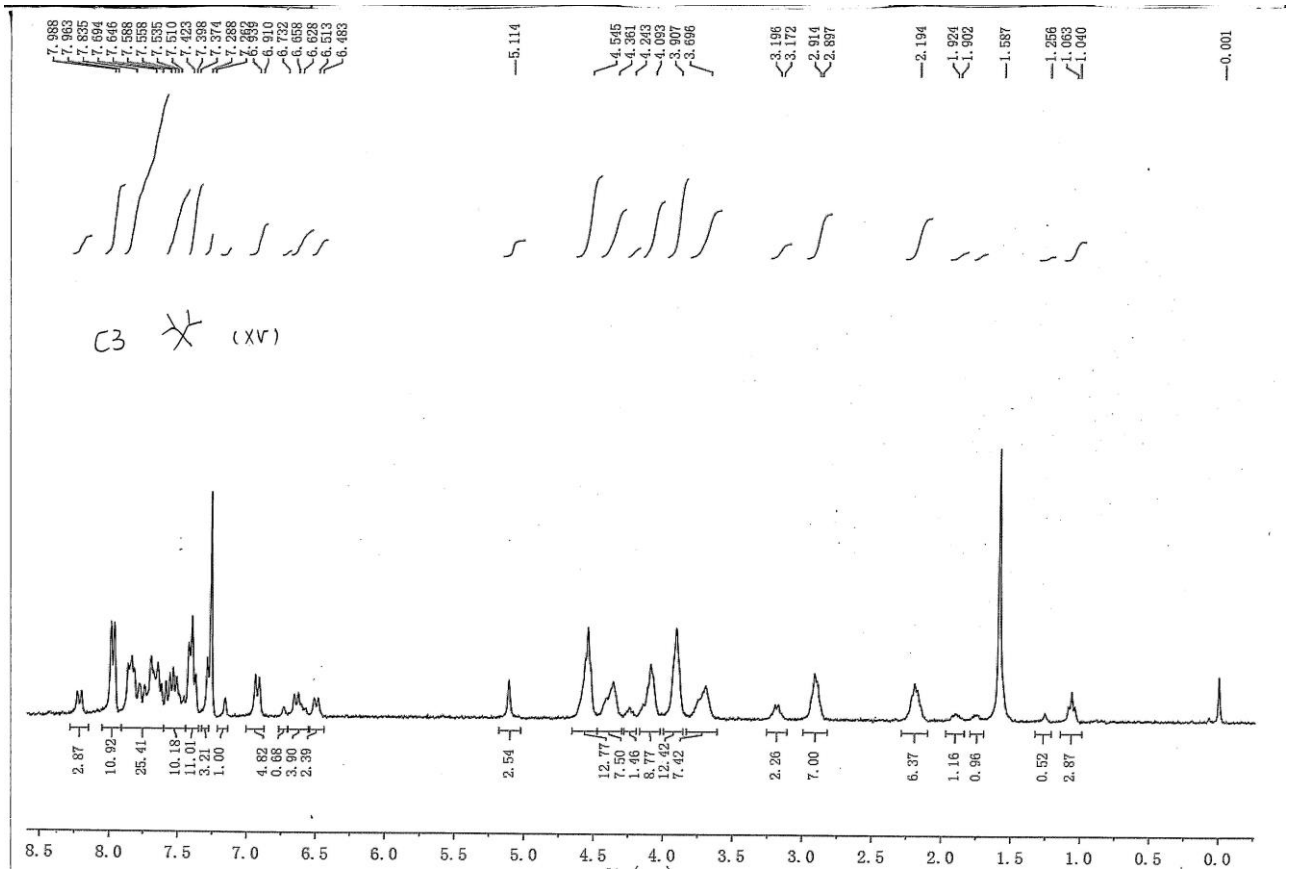

Fig.S7. ^{1}H NMR spectrum of compound **C3** in chloroform-*d*.

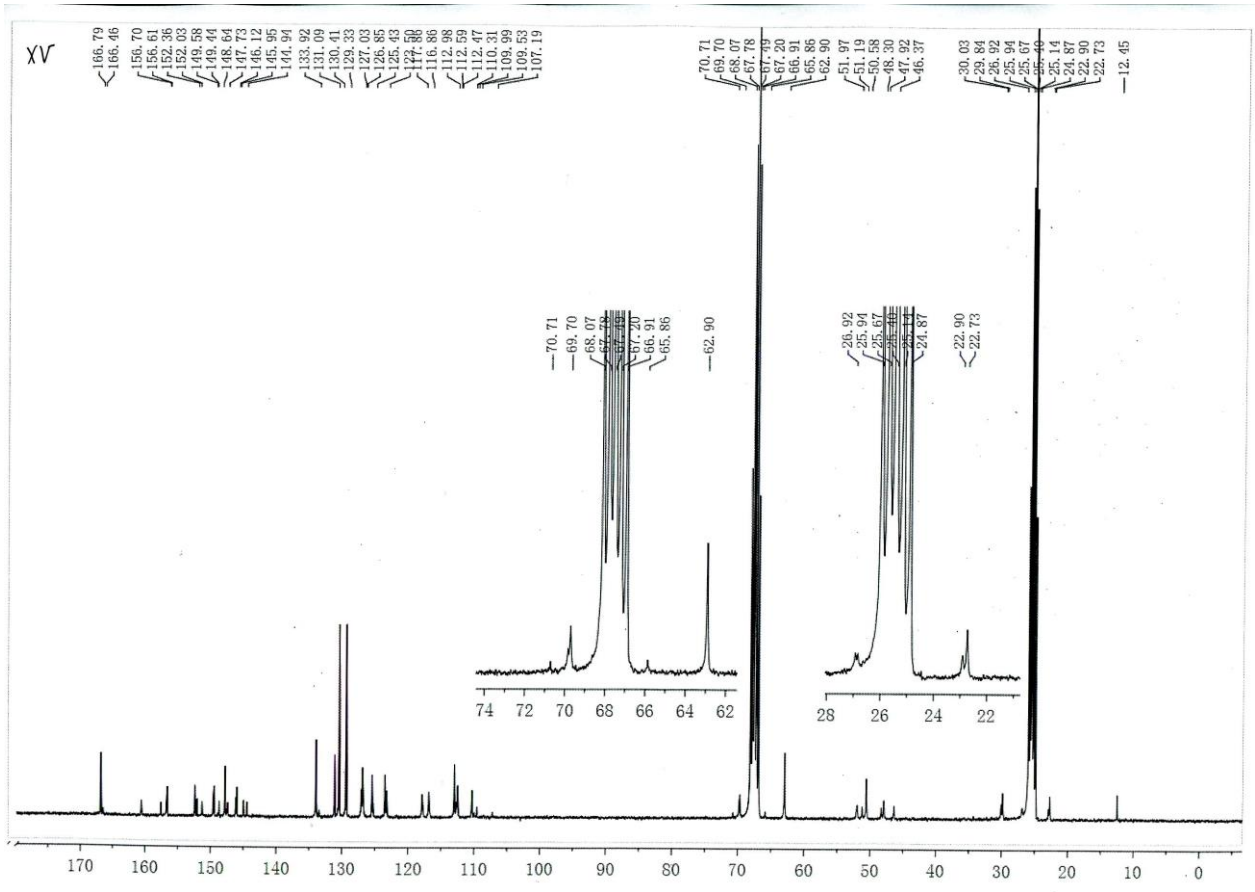

Fig.S8. ^{13}C NMR spectrum of compound **C3** in THF- d_8.

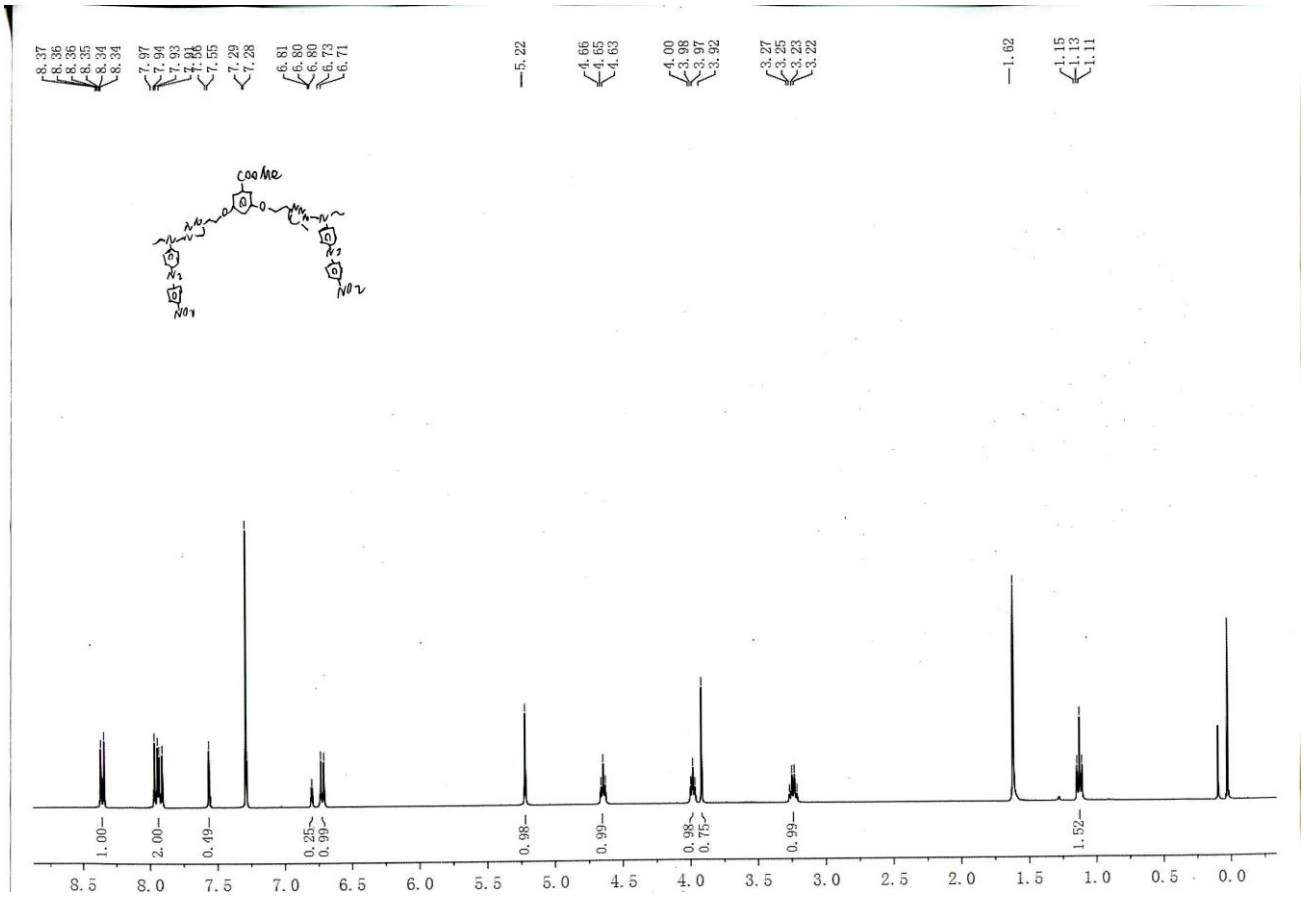

Fig.S9. ^{1}H NMR spectrum of compound **C4** in chloroform-*d*.

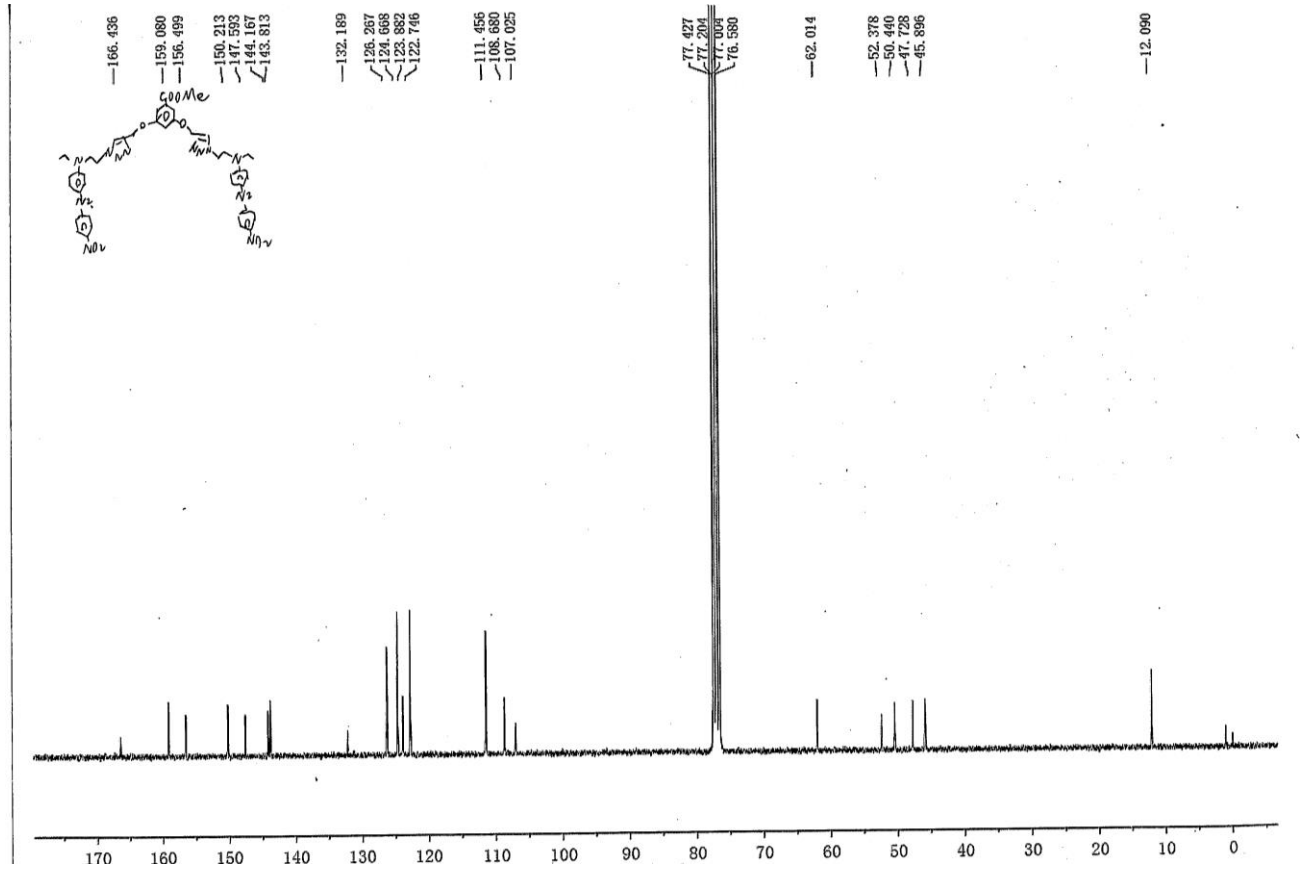

Fig.S10. ^{13}C NMR spectrum of compound **C4** in chloroform- d_8.

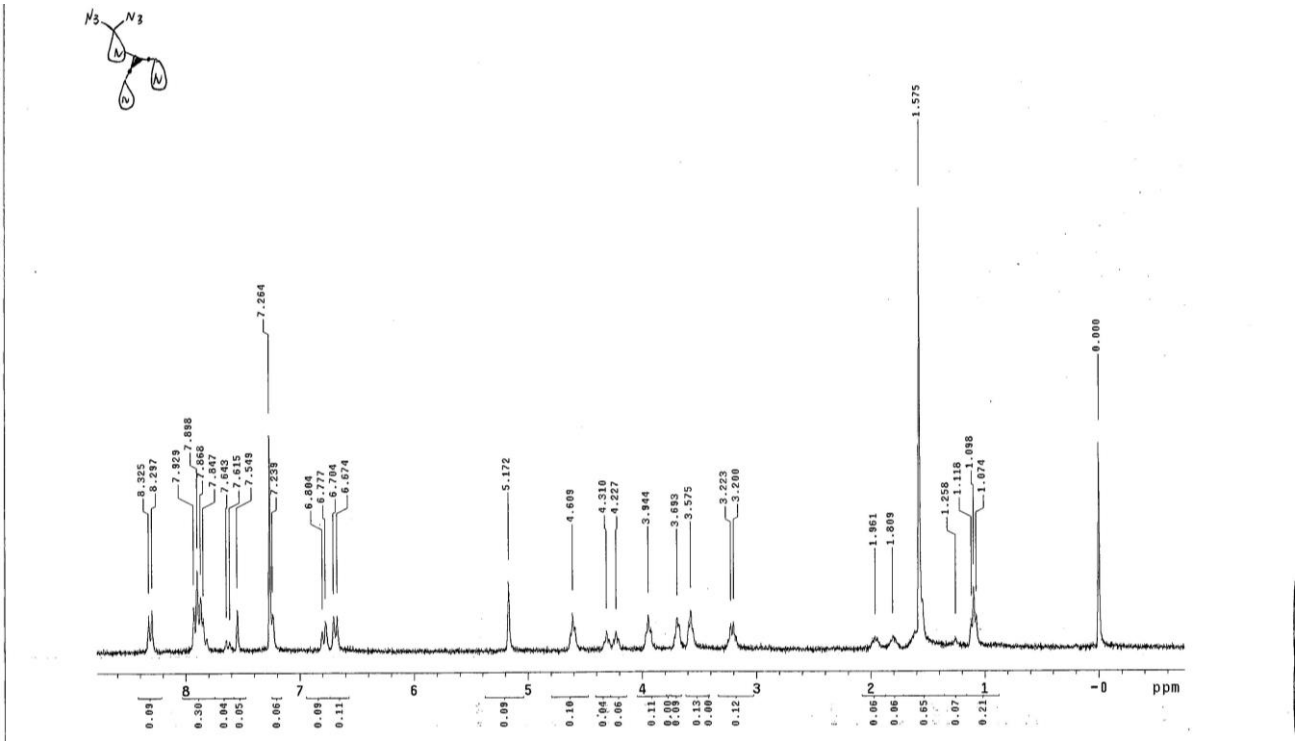

Fig.S11. ^{1}H NMR spectrum of compound **4** in chloroform-*d*.

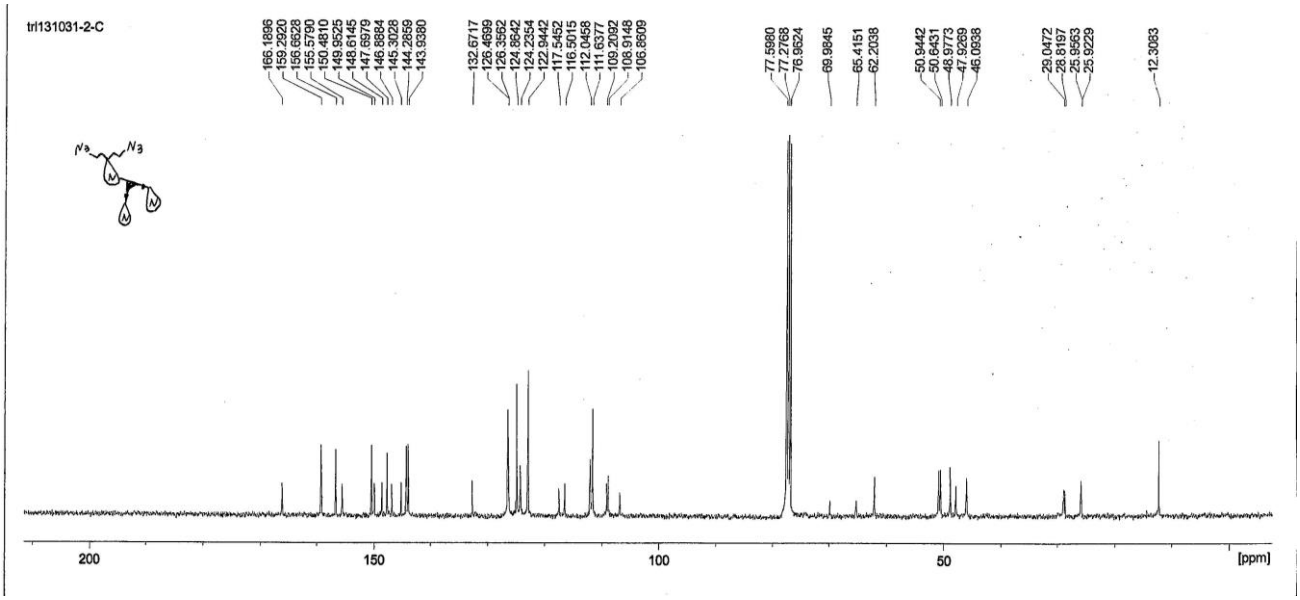

Fig.S12. ^{13}C NMR spectrum of compound **4** in chloroform-*d*.

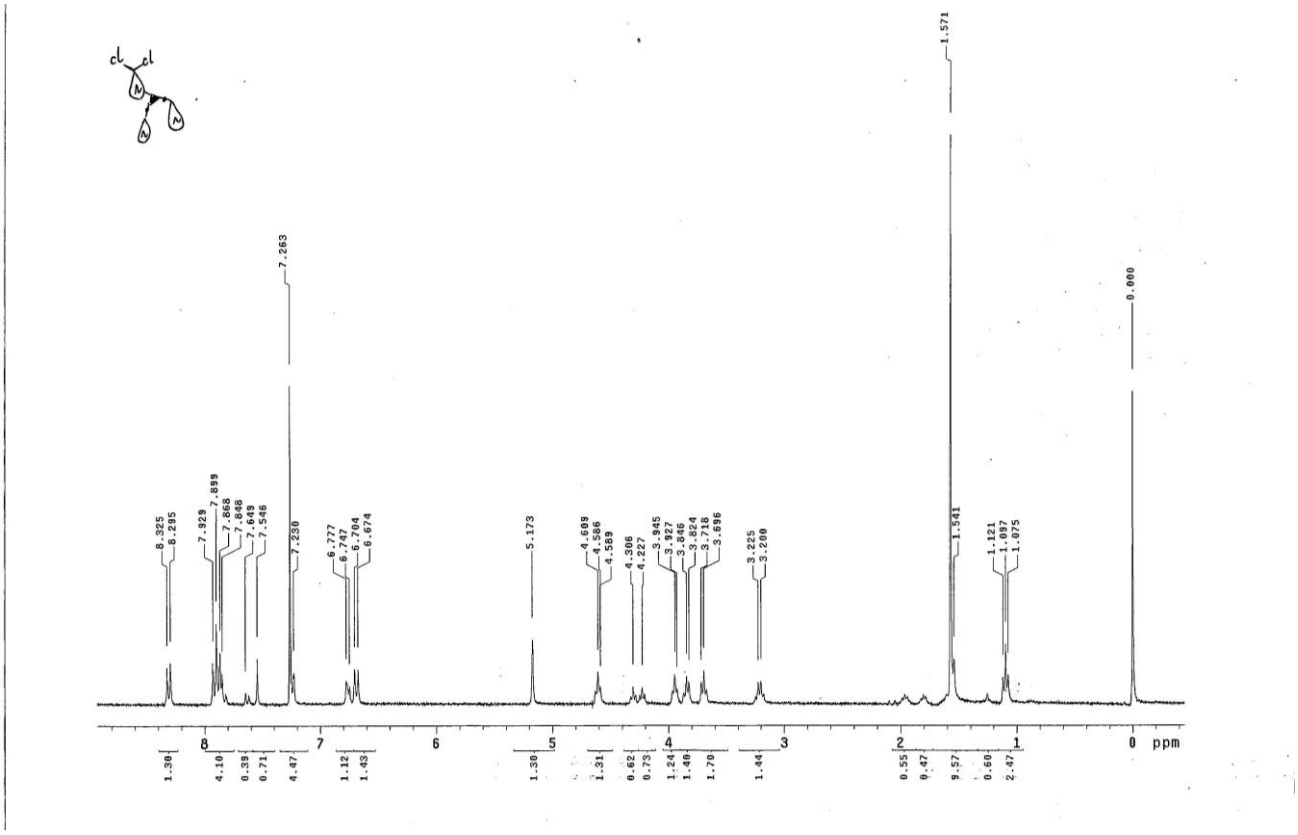

Fig.S13. ^{1}H NMR spectrum of compound **3** in chloroform-*d*.

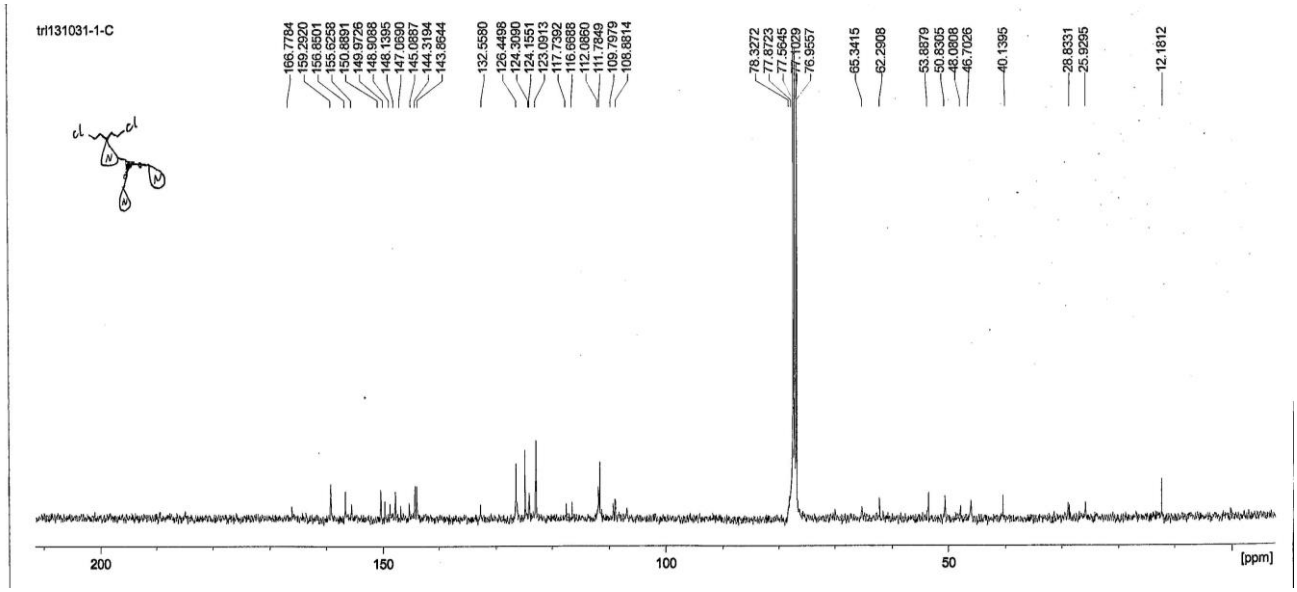

Fig.S14. ^{13}C NMR spectrum of compound **3** in chloroform-*d*.

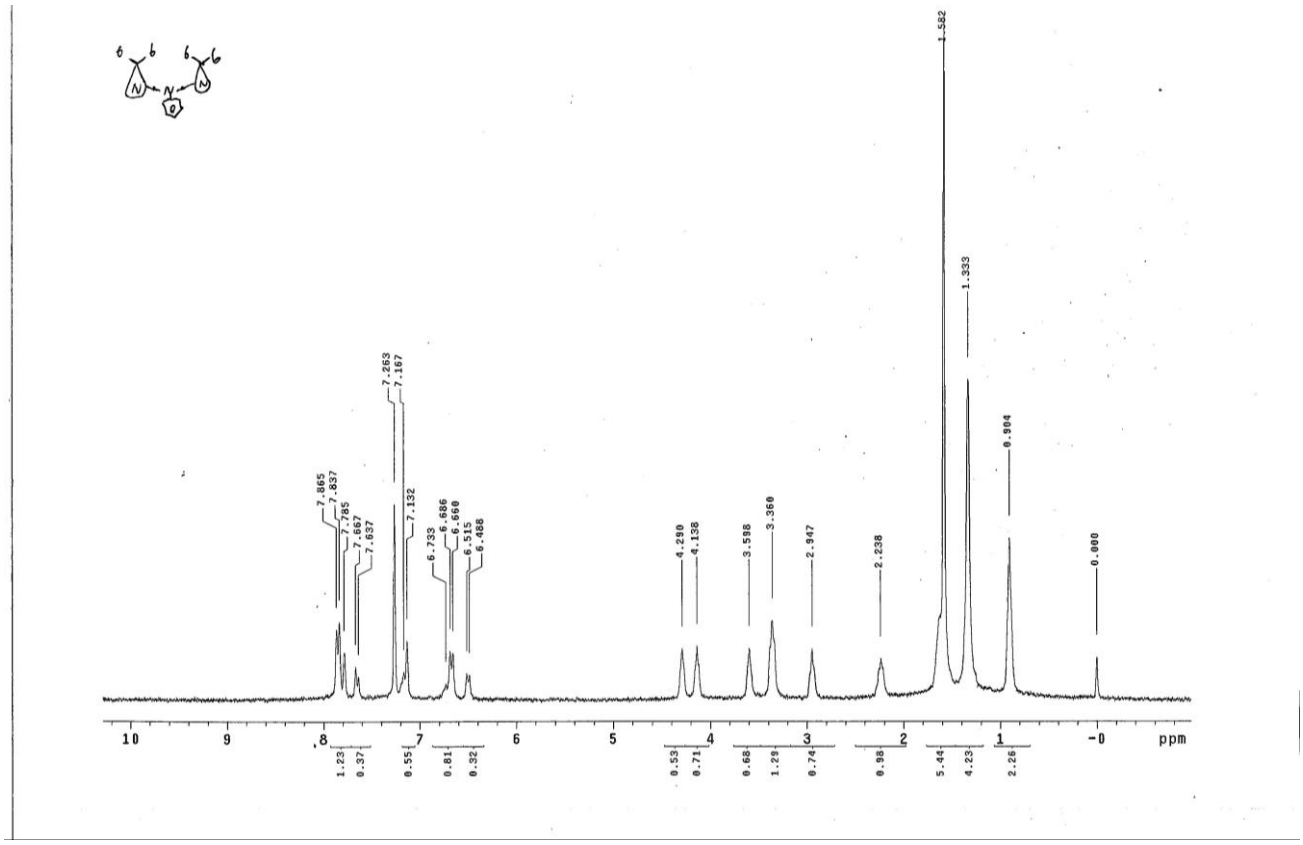

Fig.S15. ^{1}H NMR spectrum of compound **5** in chloroform-*d*.

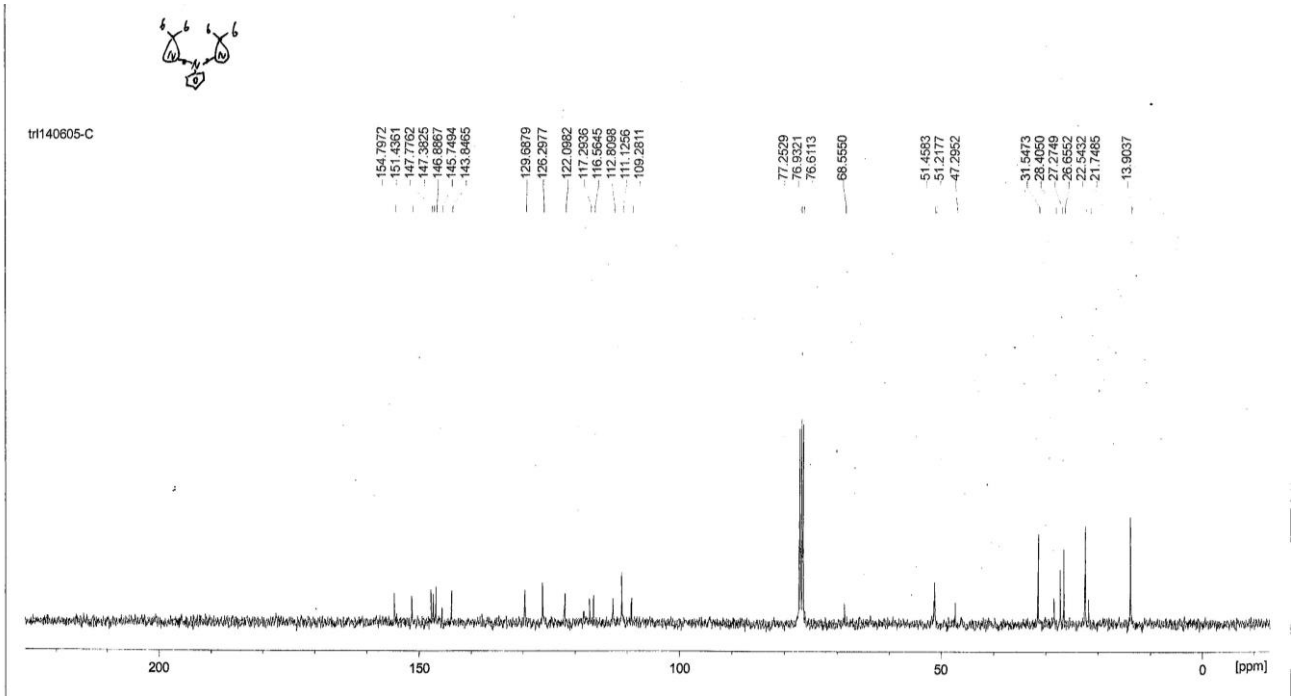

Fig.S16. ^{13}C NMR spectrum of compound **5** in chloroform-*d*.

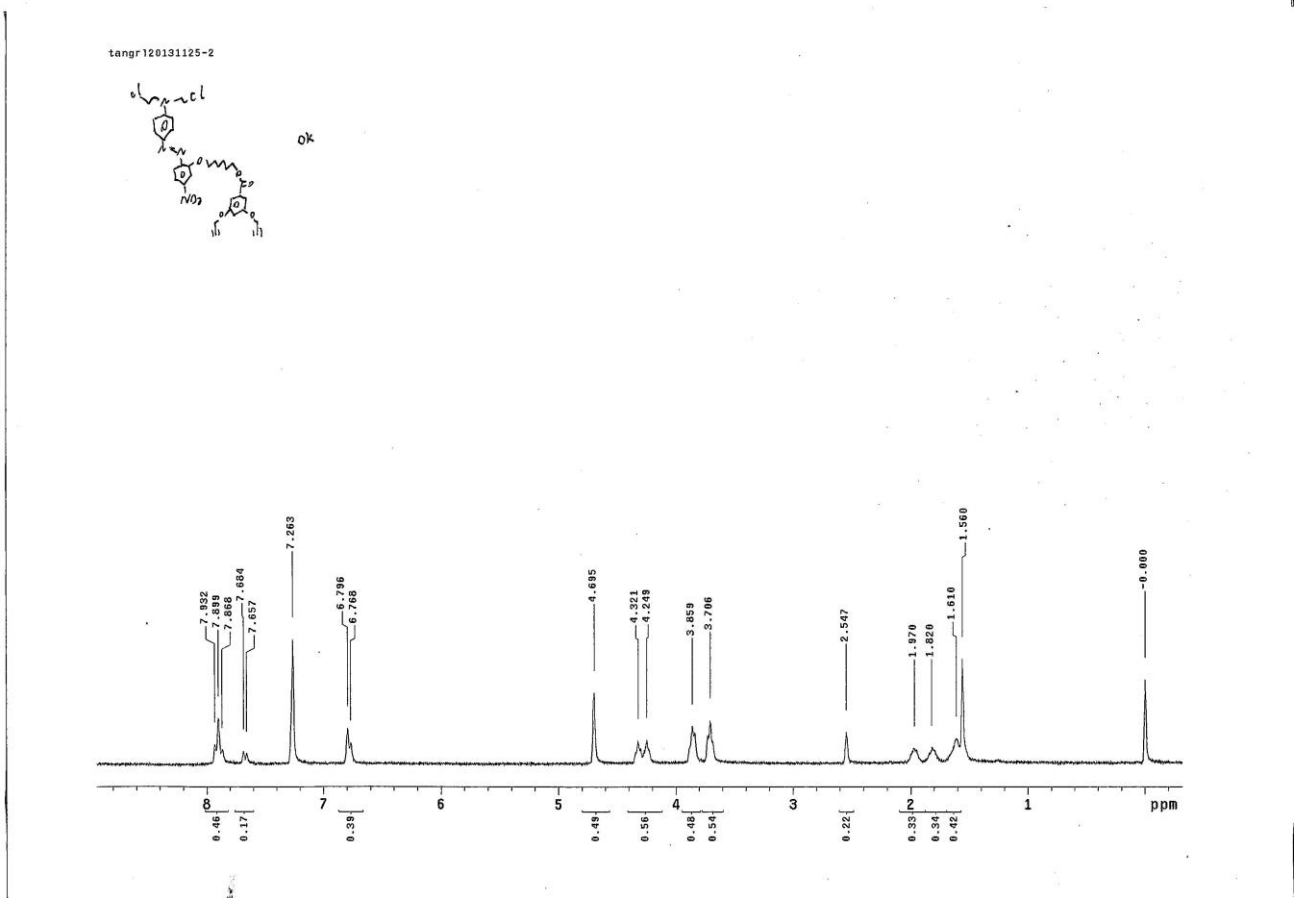

Fig.S17. ^{1}H NMR spectrum of compound **1** in chloroform-*d*.

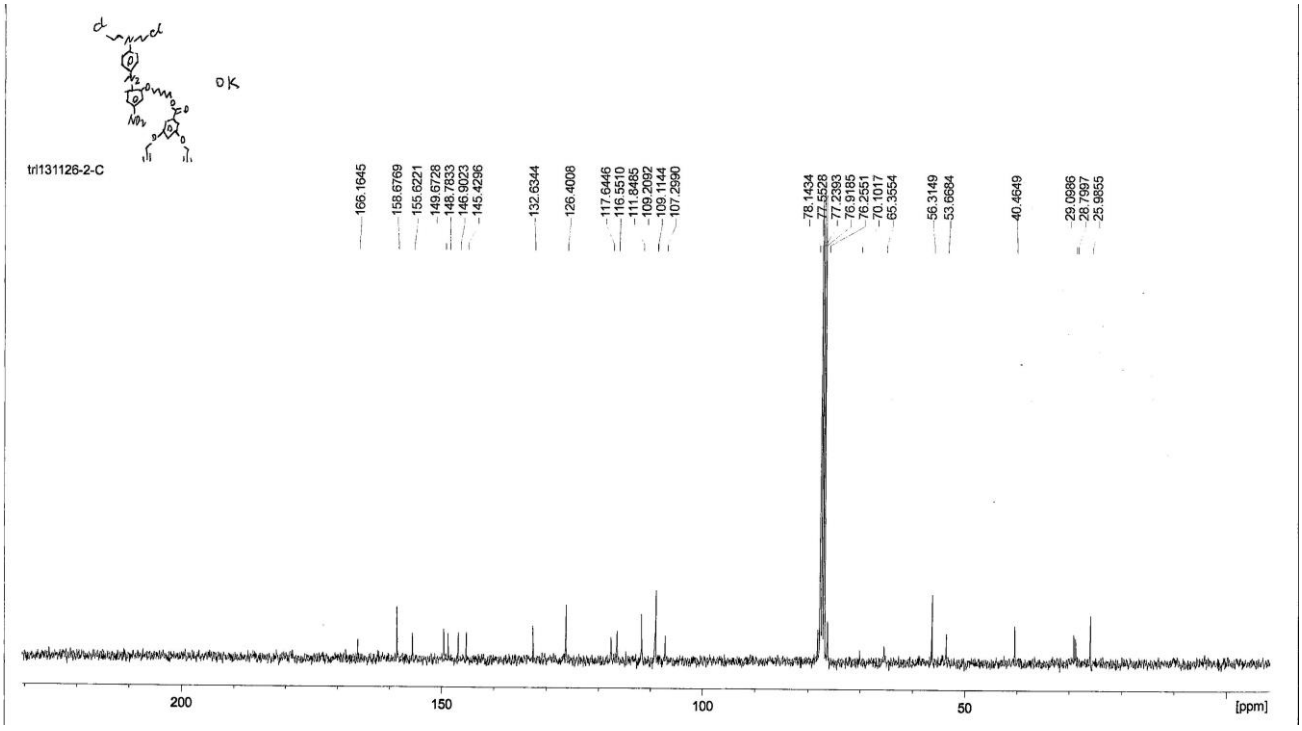

Fig.S18. ^{13}C NMR spectrum of compound **1** in chloroform-*d*.

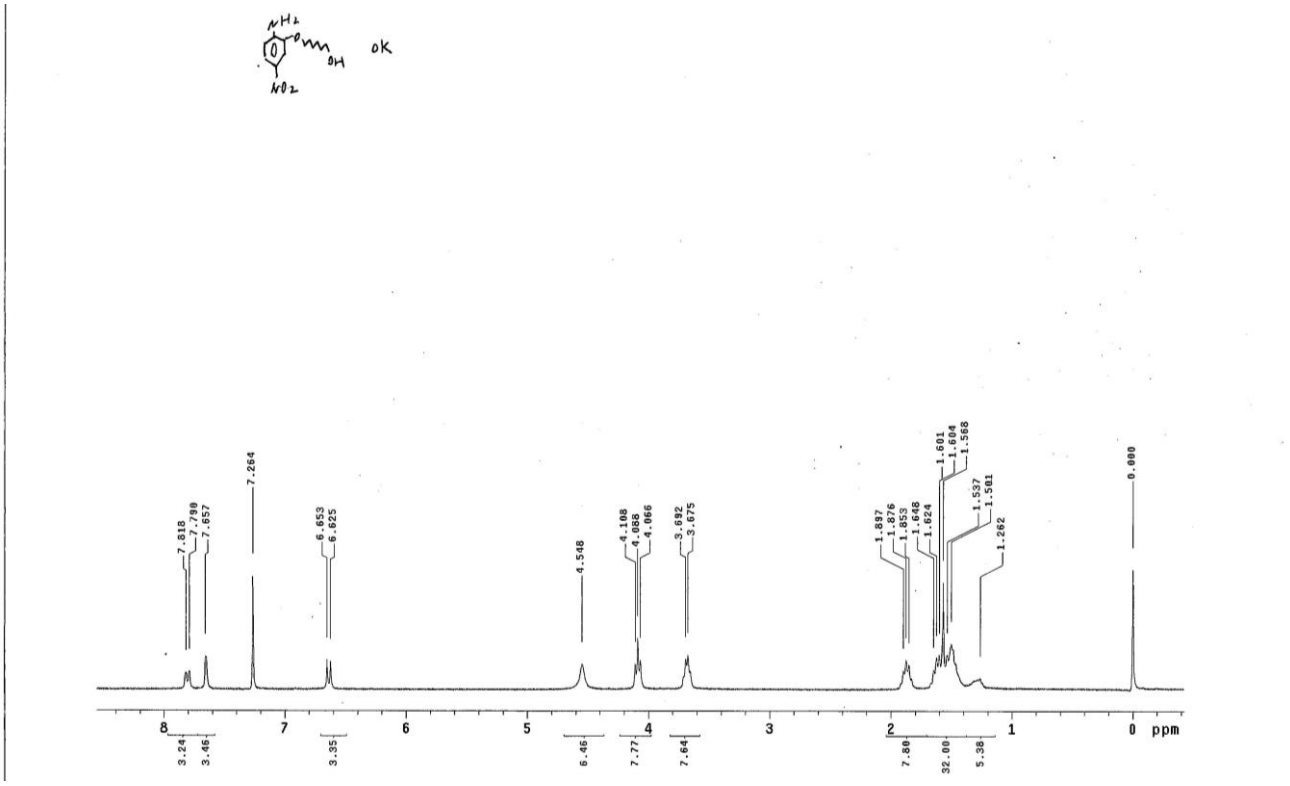

Fig.S19. ^{1}H NMR spectrum of compound **8** in chloroform-*d*.

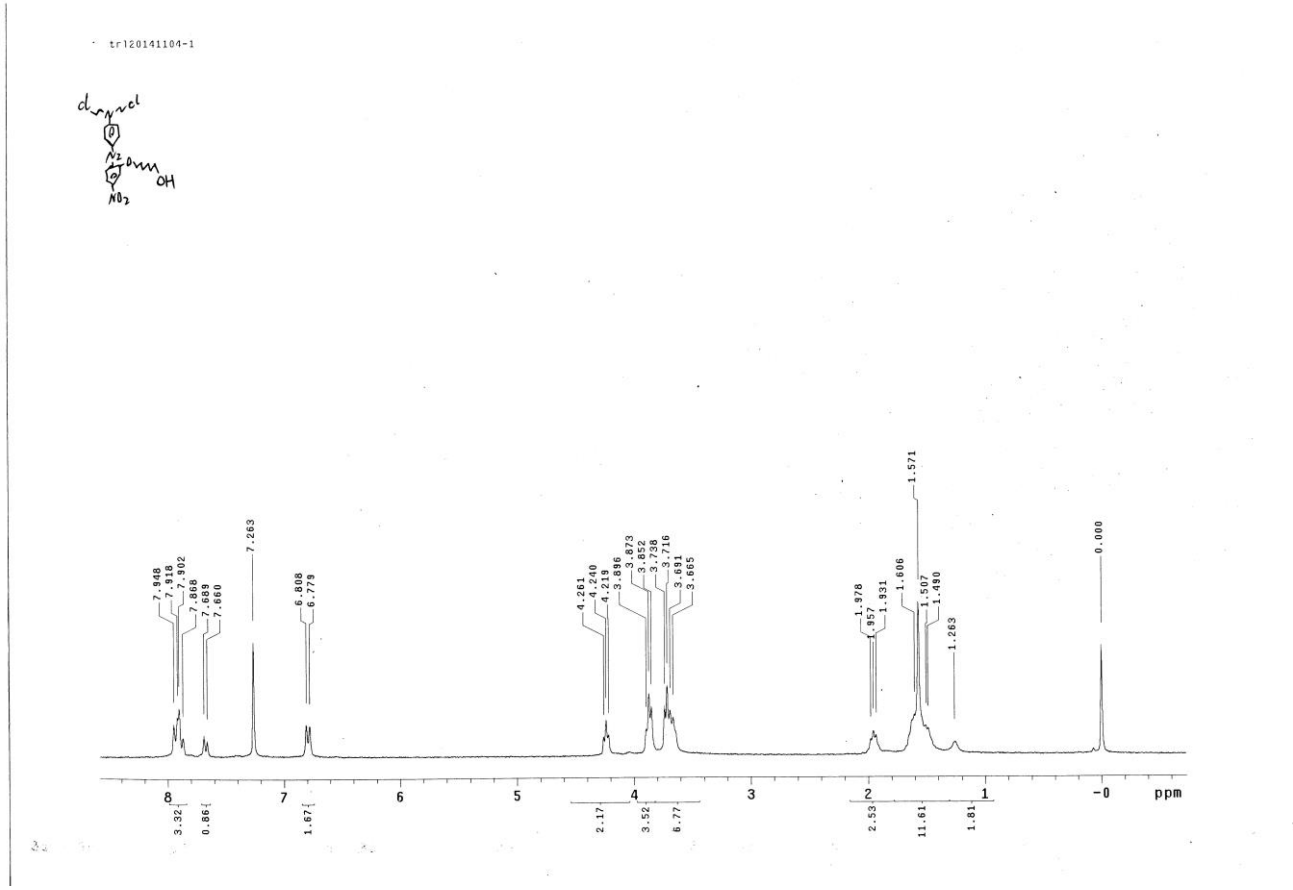

Fig.S20. ^{1}H NMR spectrum of compound **8** in chloroform-*d*.

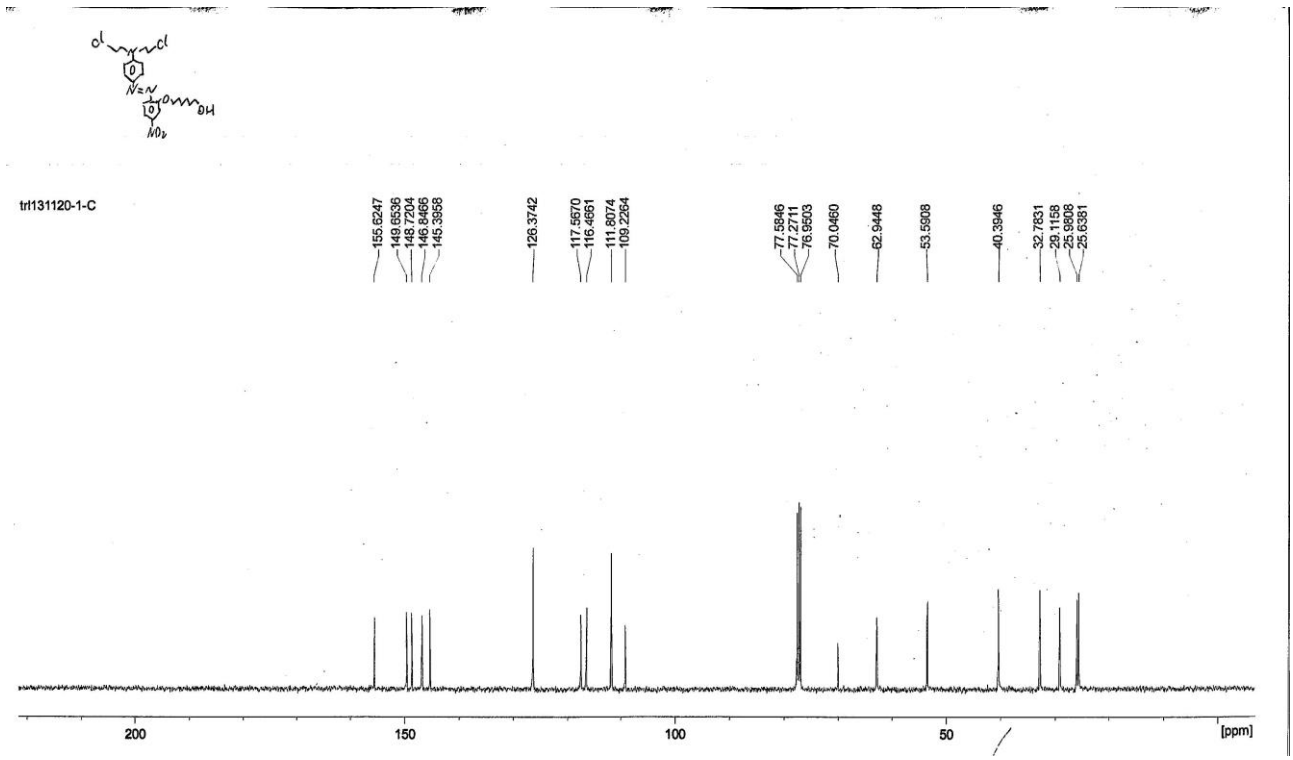

Fig.S21. ^{13}C NMR spectrum of compound **8** in chloroform-*d*.

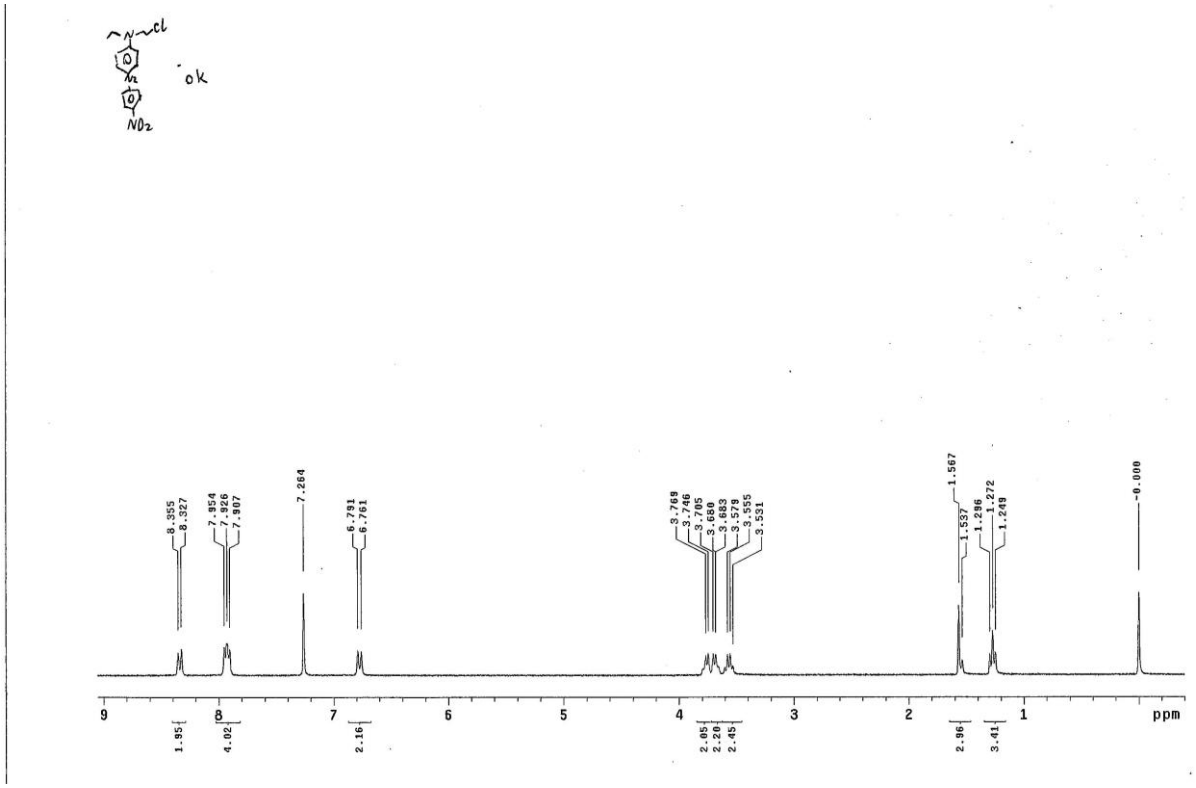

Fig.S22. ^{1}H NMR spectrum of compound **12** in chloroform-*d*.

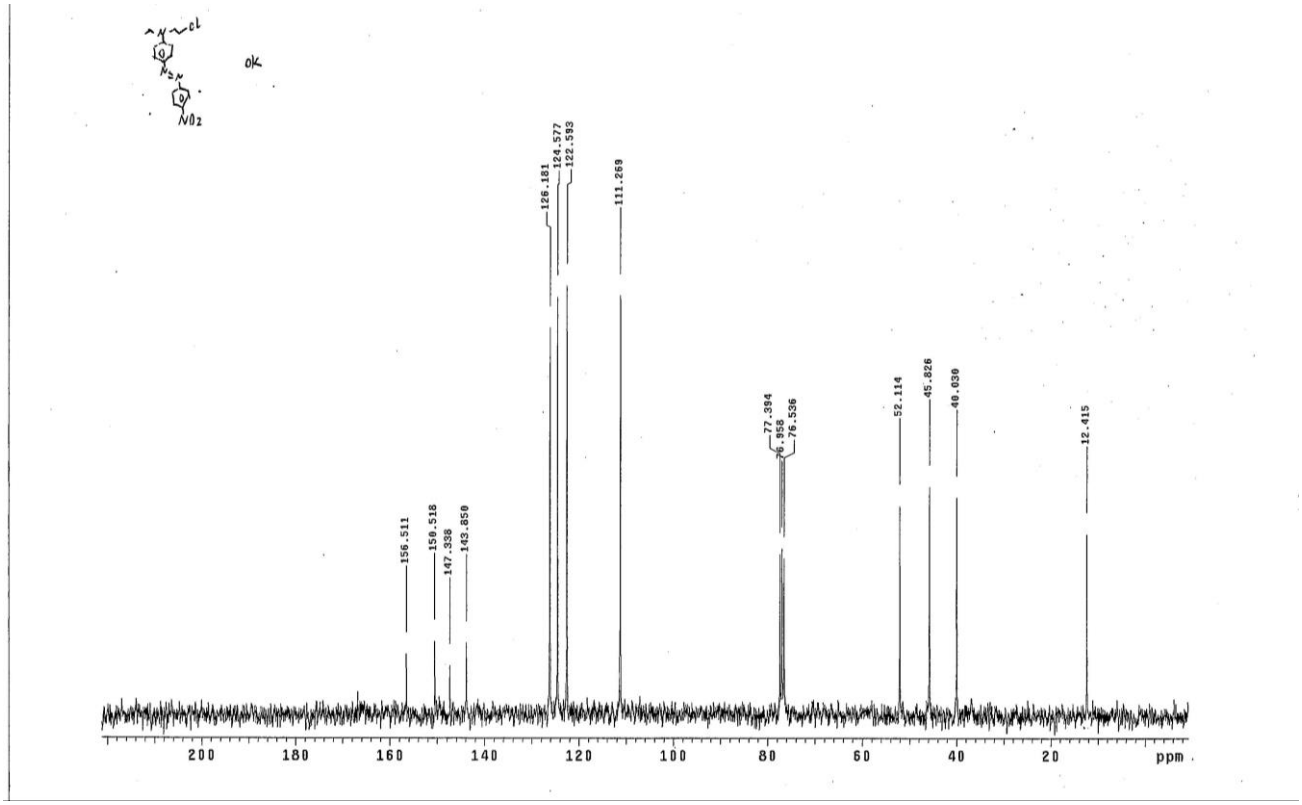

Fig.S23. ^{13}C NMR spectrum of compound **12** in chloroform-*d*.

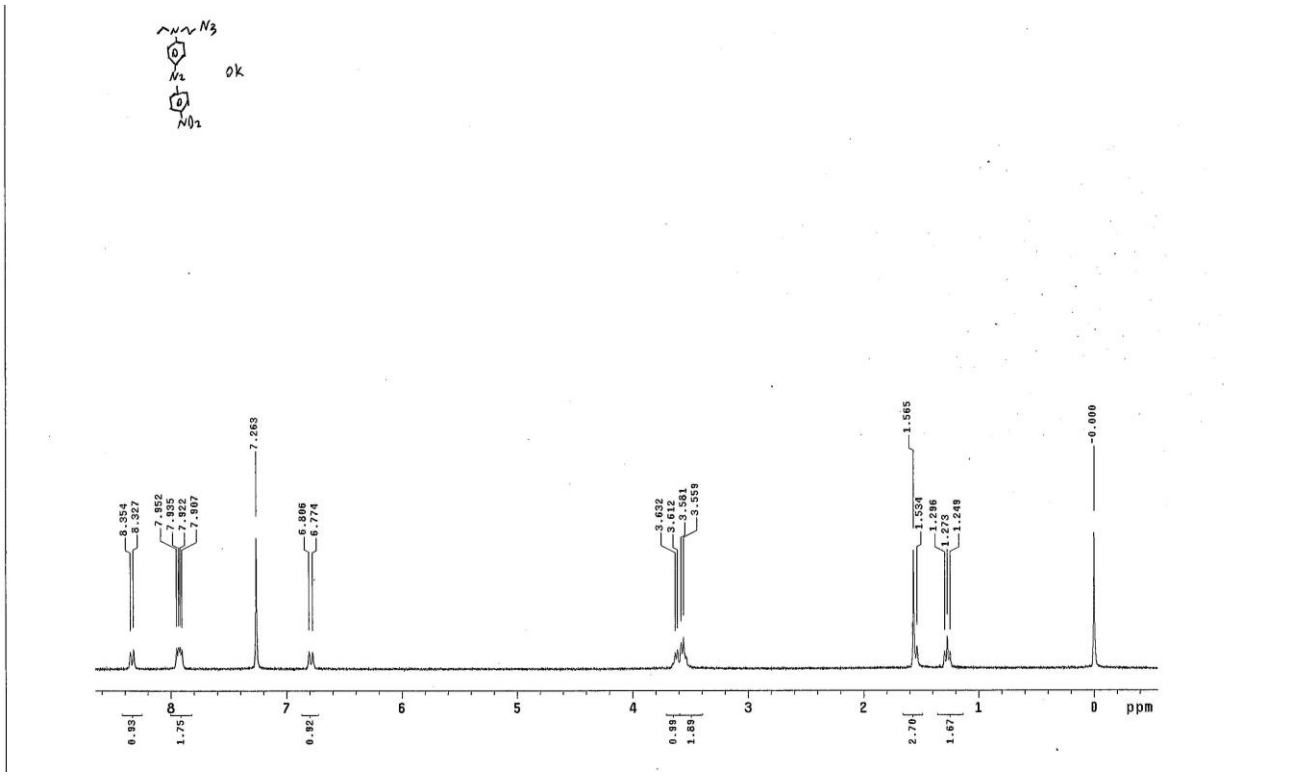

Fig.S24. ^{1}H NMR spectrum of compound **2** in chloroform-*d*.

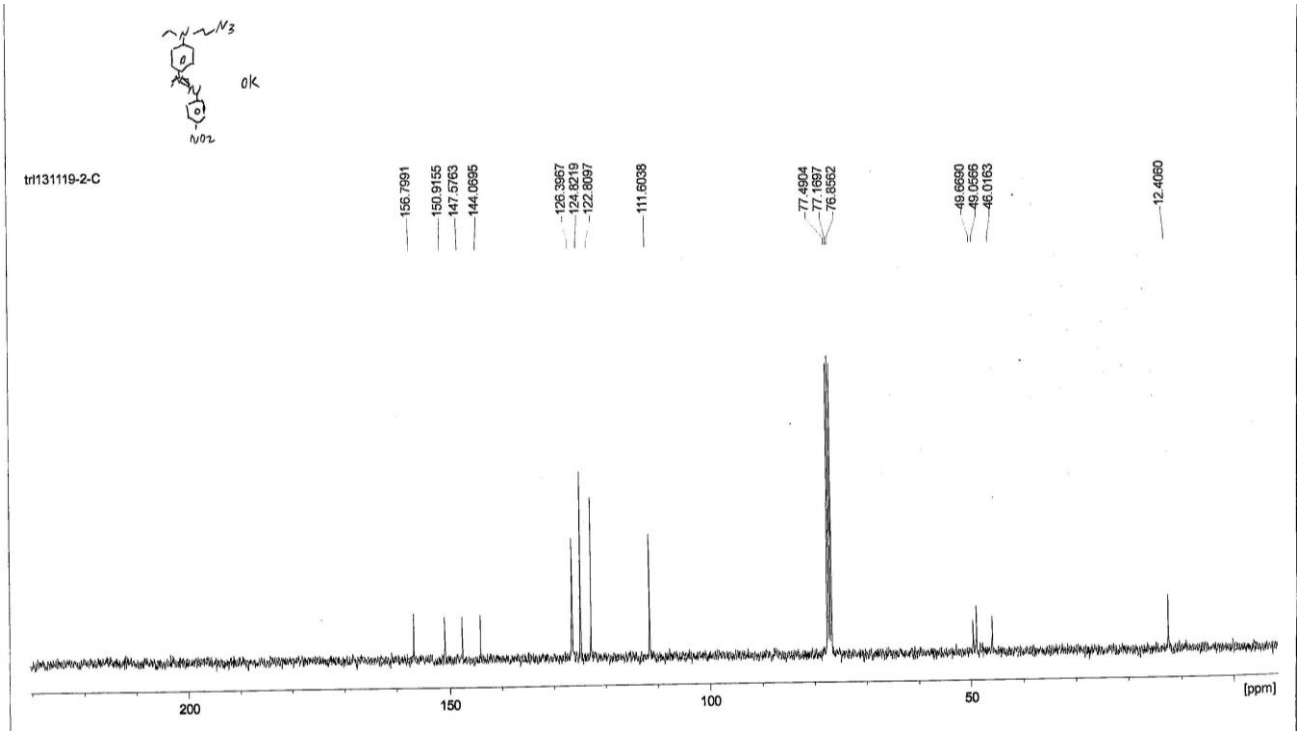

Fig.S25. ^{13}C NMR spectrum of compound **2** in chloroform-*d*.

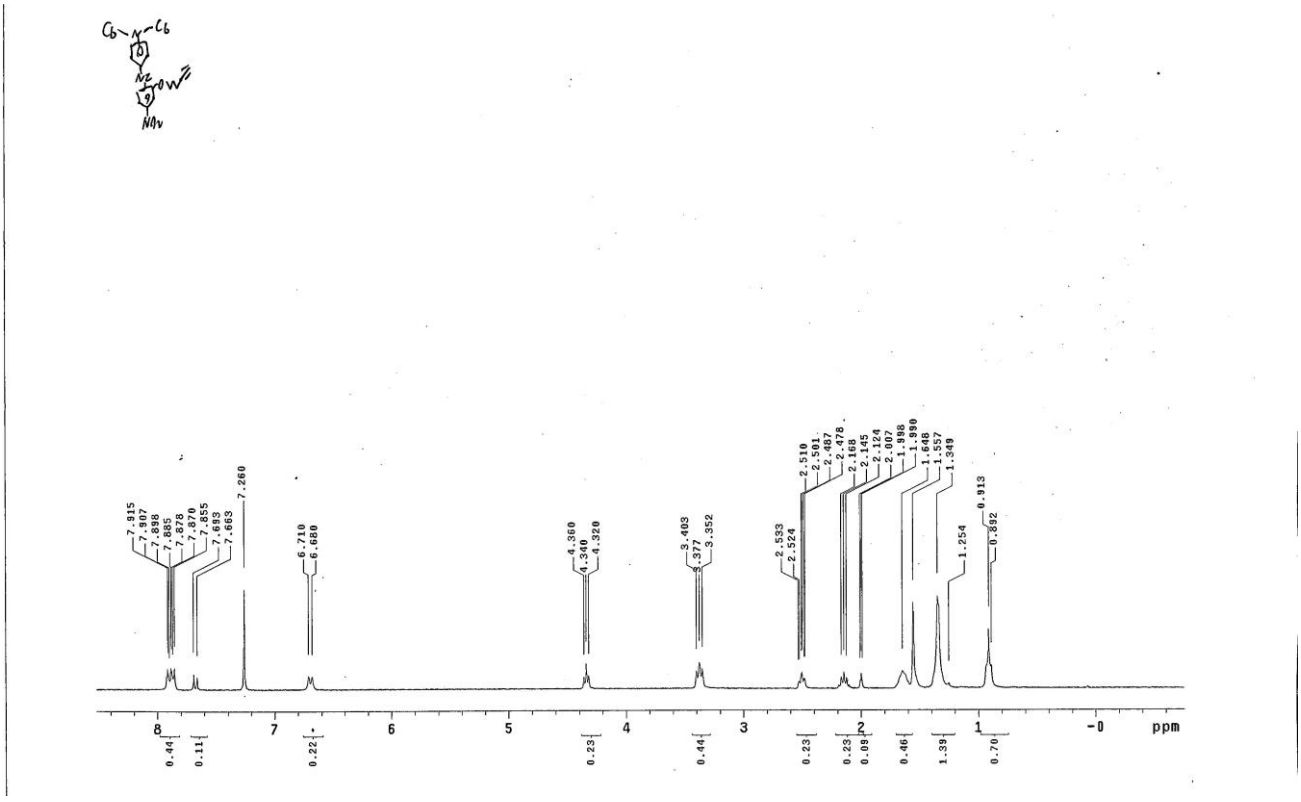

Fig.S26. ^{1}H NMR spectrum of compound **6** in chloroform-*d*.

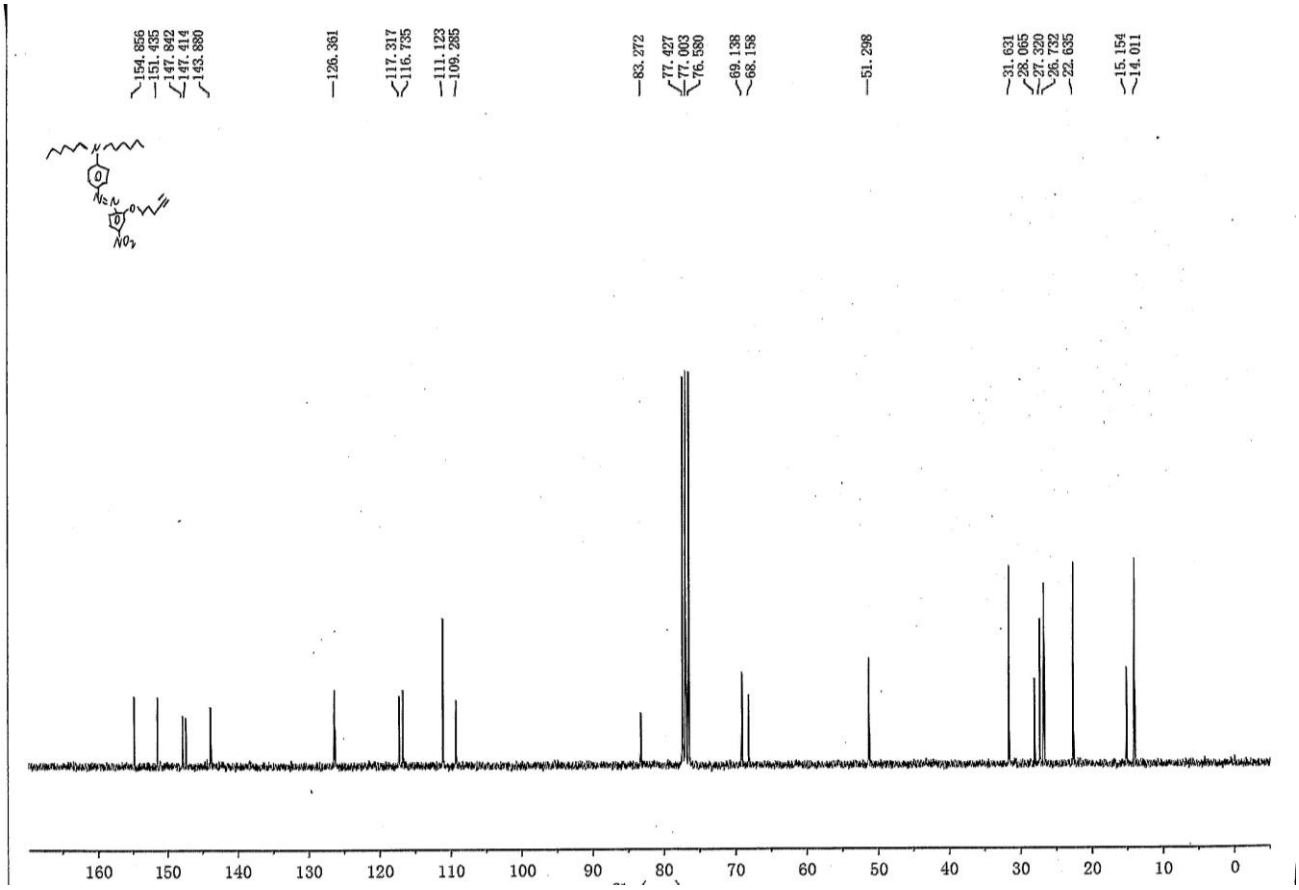

Fig.S27. ^{13}C NMR spectrum of compound **6** in chloroform-*d*.

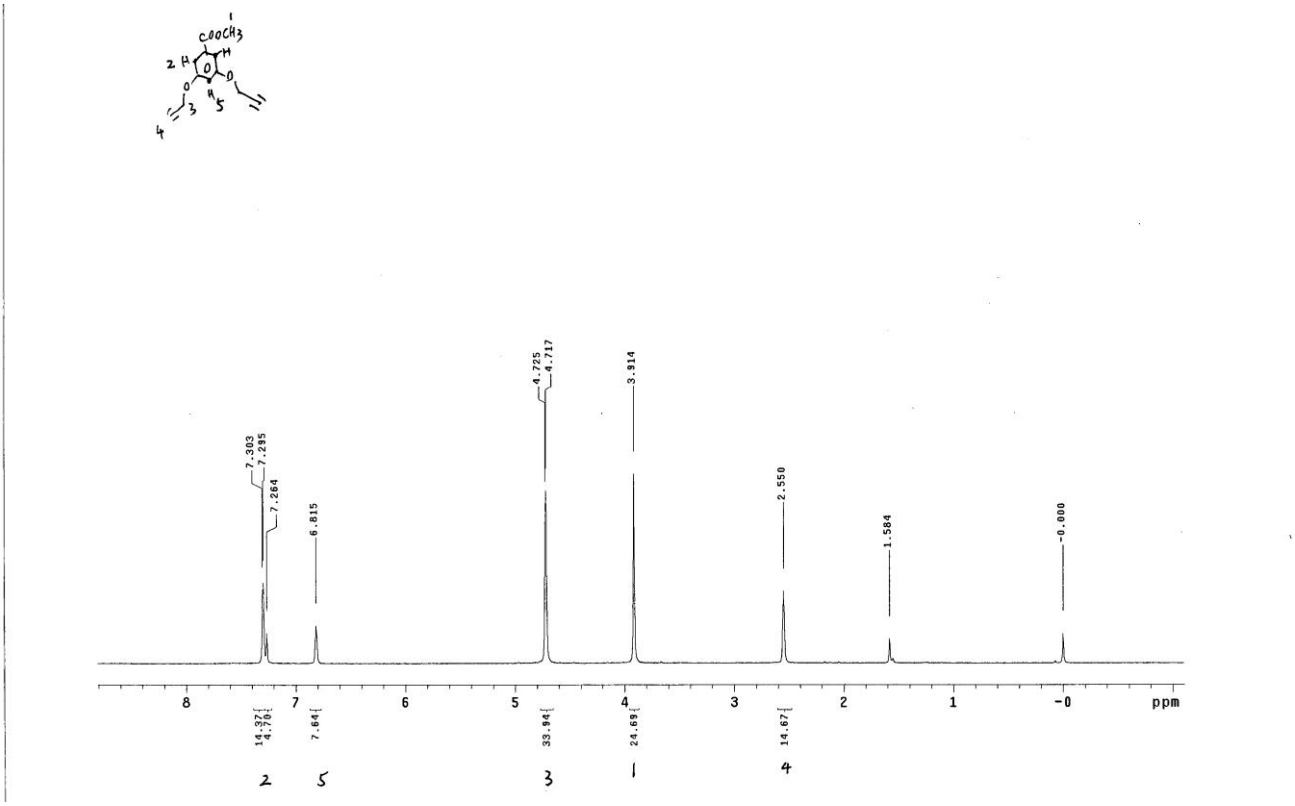

Fig.S28. ^{1}H NMR spectrum of compound **13** in chloroform-*d*.

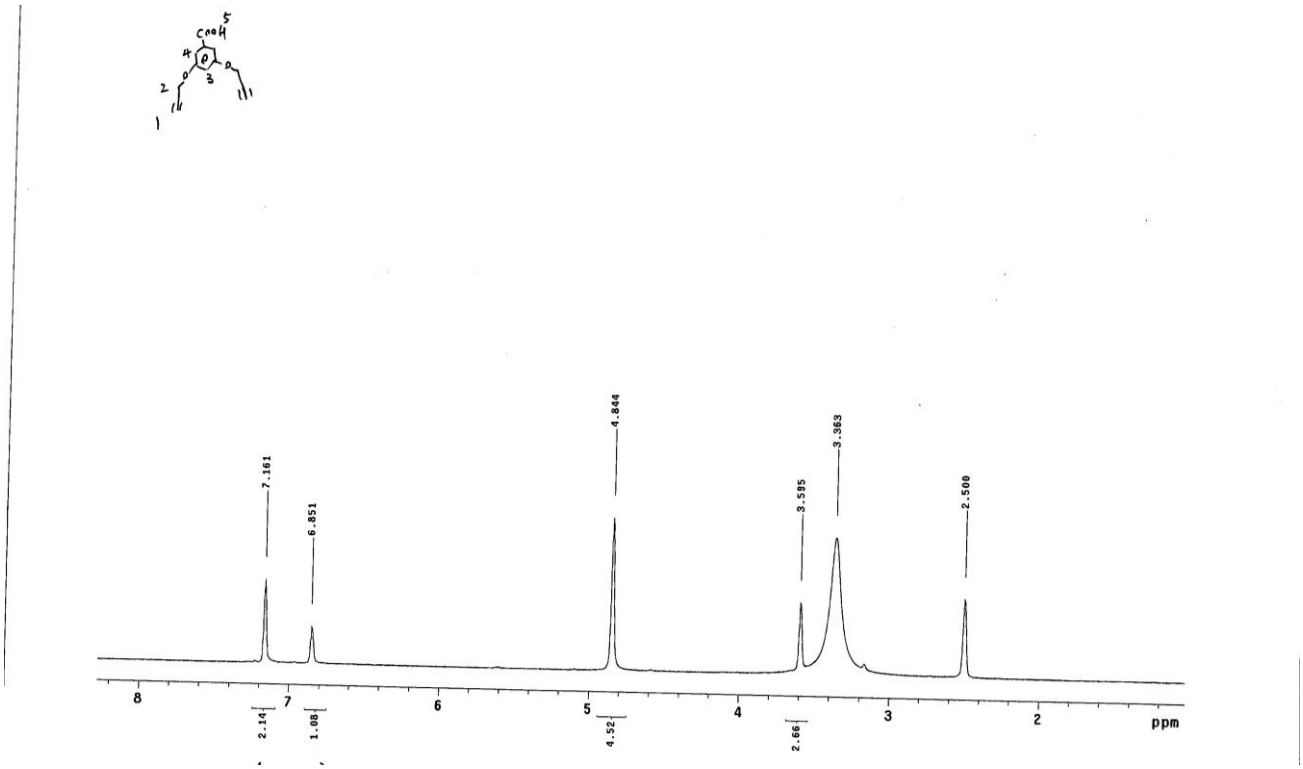

Fig.S29. ^{1}H NMR spectrum of compound **9** in chloroform-*d*

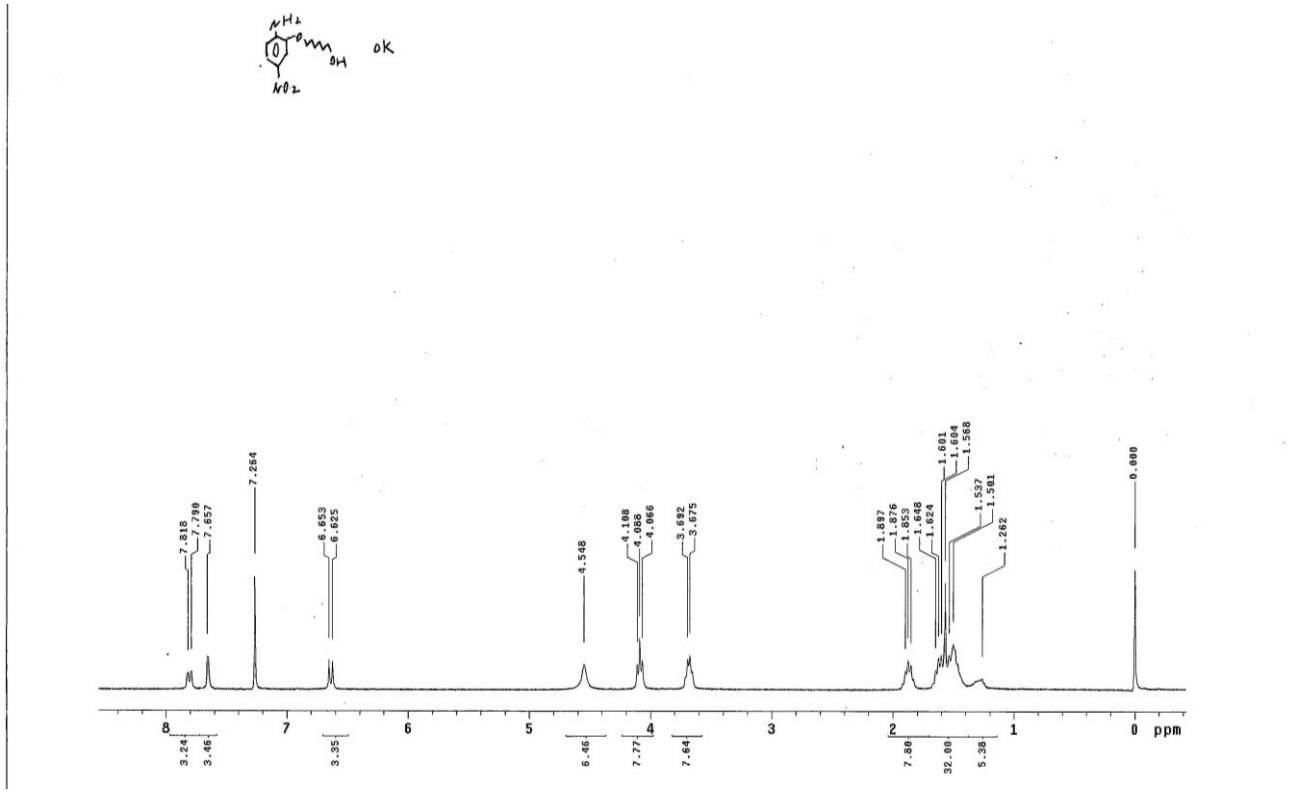

Fig.S30. ^{1}H NMR spectrum of compound **7** in chloroform-*d*.

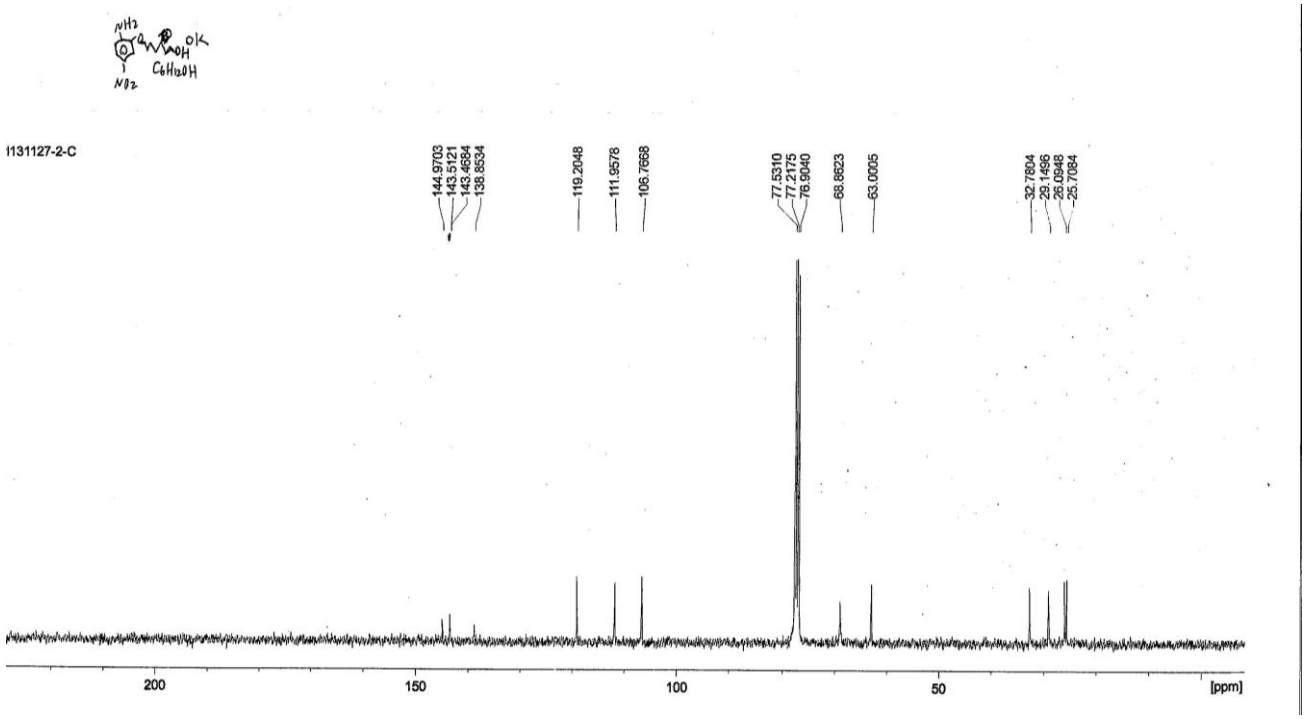

Fig.S31. ^{13}C NMR spectrum of compound **7** in chloroform-*d*.

The MALDI-TOF Mass spectra of C1-C3:

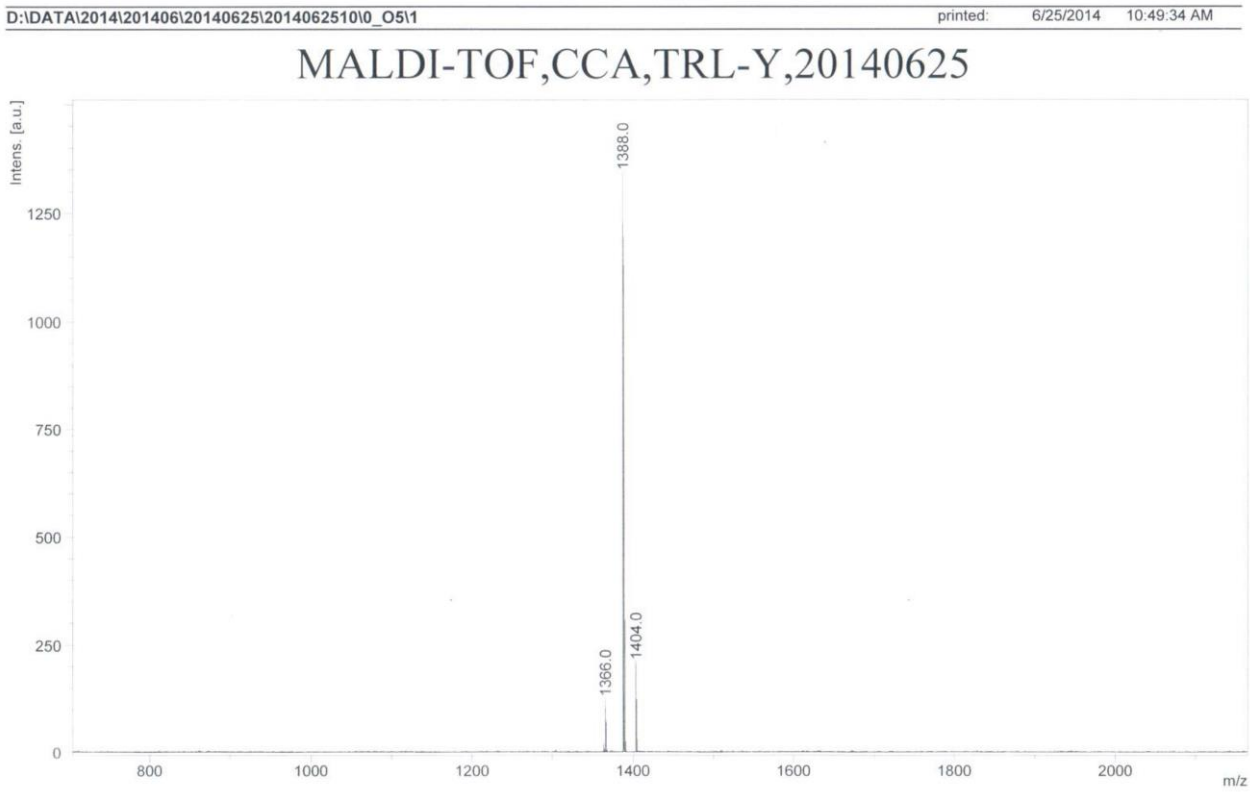

Fig.S32. The MALDI-TOF mass spectrum of compound **C1**.

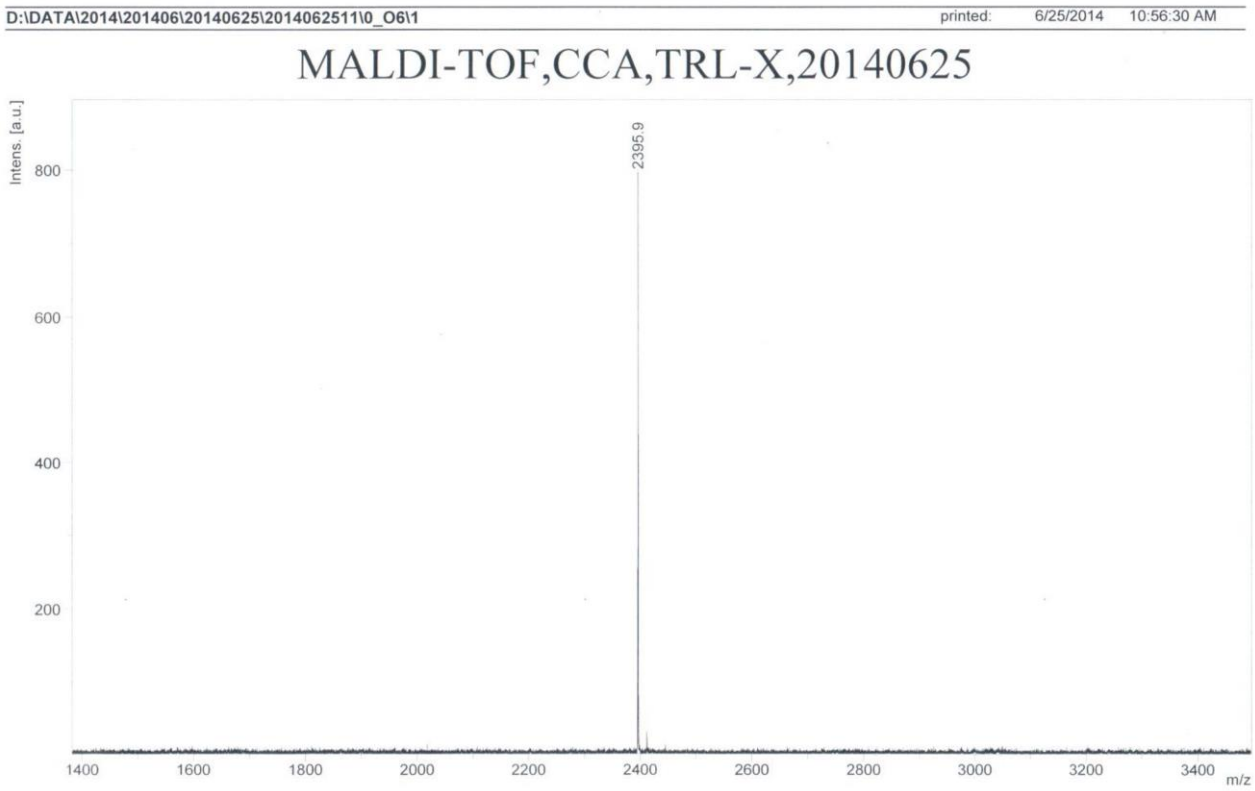

Fig.S33. The MALDI-TOF mass spectrum of compound **C2**.

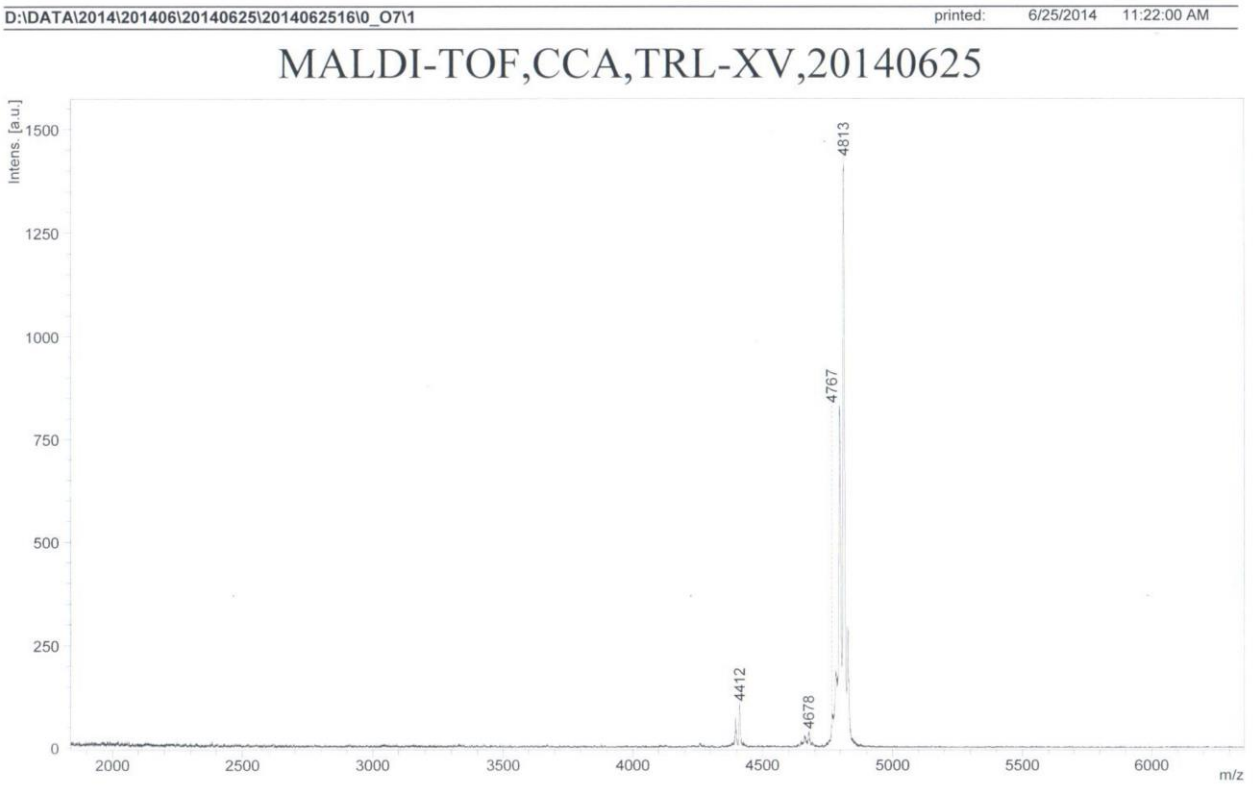

Fig.S34. The MALDI-TOF mass spectrum of compound **C3**.

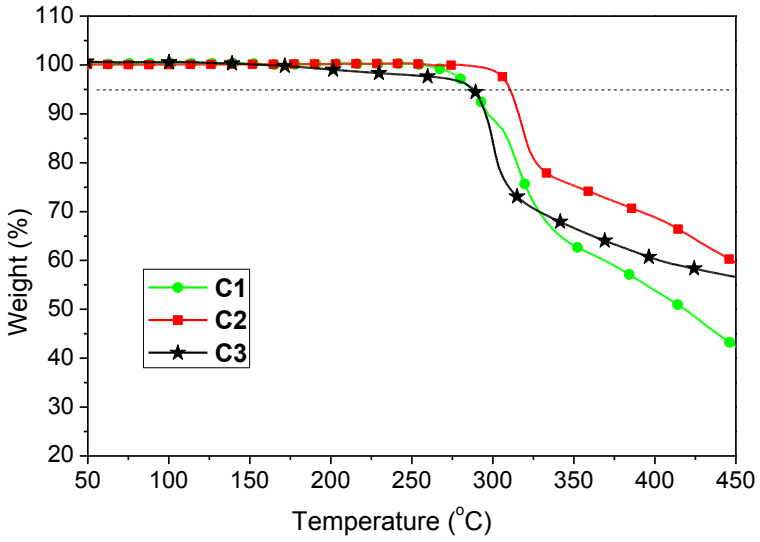

Fig. S35. TGA thermograms of **C1**- **C3** measured in nitrogen at a heating rate of 10 ℃/min.

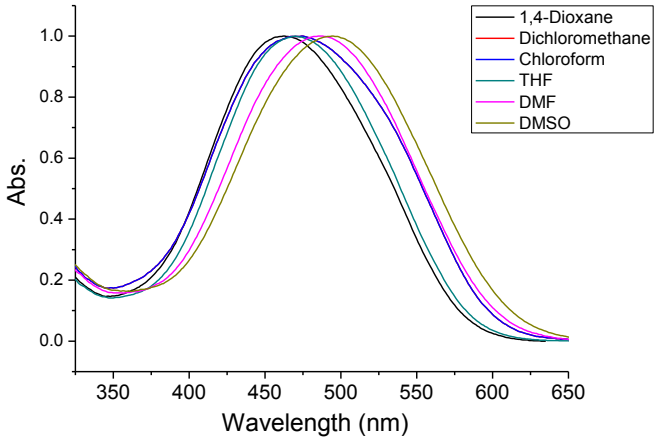

Fig. S36. UV-vis absorption spectra of **C1** in different solvents.

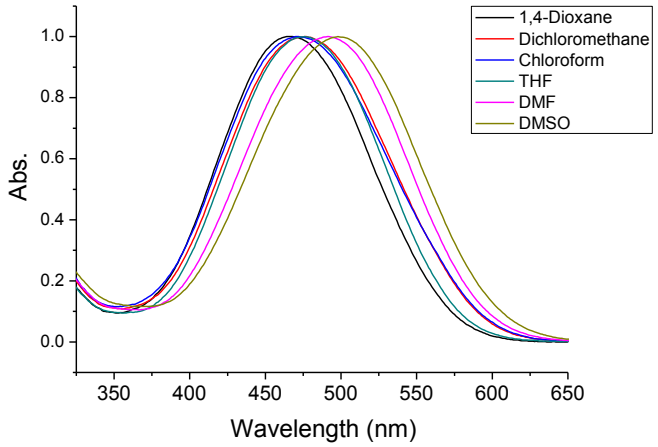

Fig. S37. UV-vis absorption spectra of **C2** in different solvents.

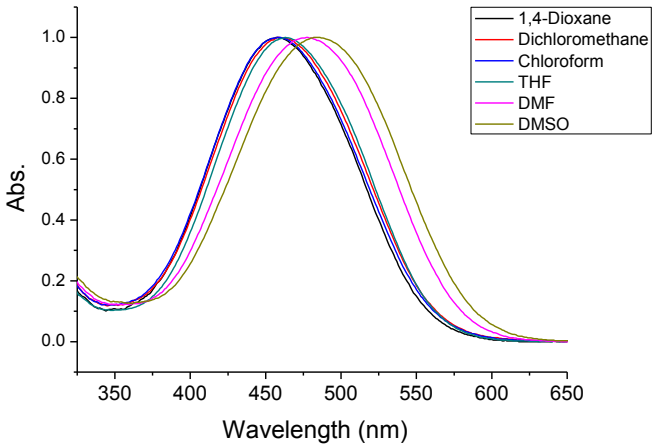

Fig. S38. UV-vis absorption spectra of **C3** in different solvents.

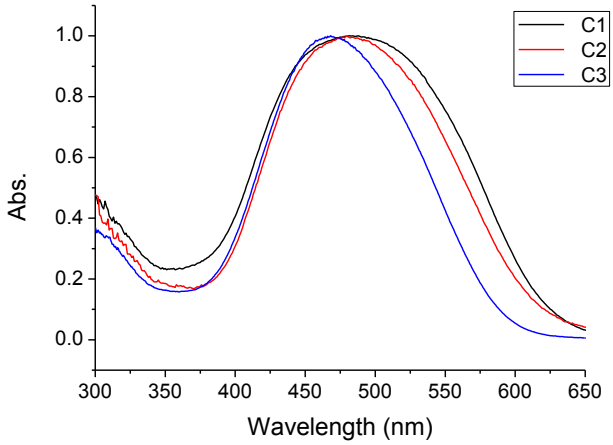

Fig. S39. UV-vis absorption spectra of thin films.

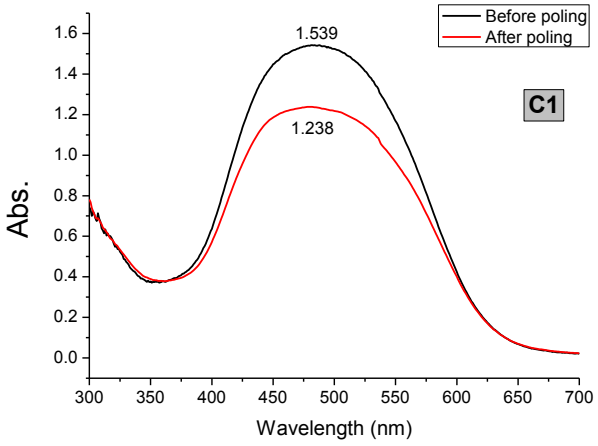

Fig. S40. UV-vis absorption spectra of thin film: **C1**, before and after poling.

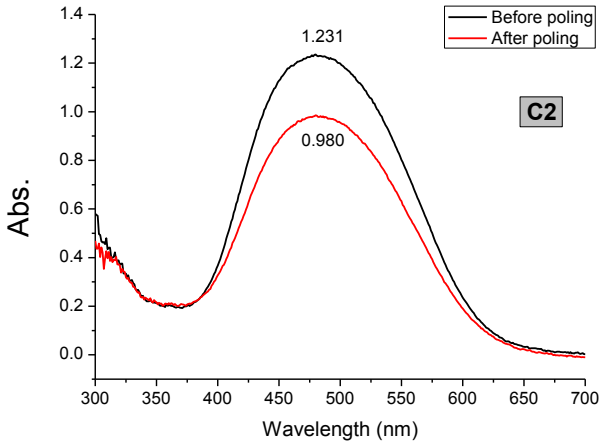

Fig. S41. UV-vis absorption spectra of thin film: **C2**, before and after poling.

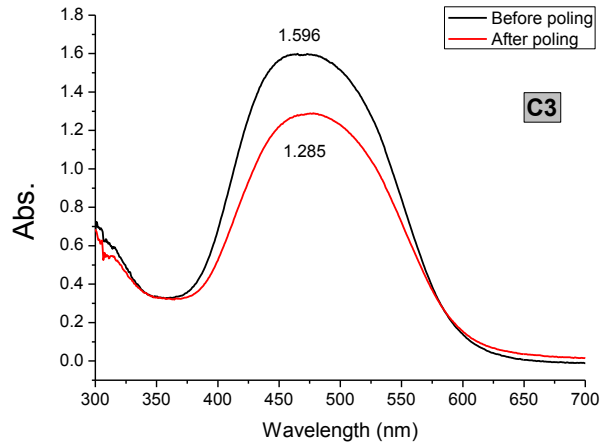

Fig. S42. UV-vis absorption spectra of thin film: **C3**, before and after poling.

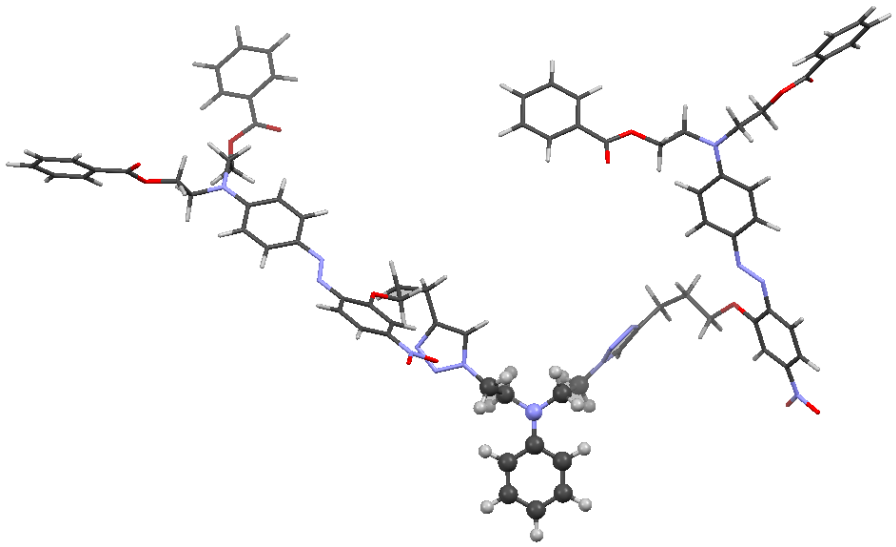

Fig. S43. The optimized structure of **G1** calculated by molecular dynamic simulation.

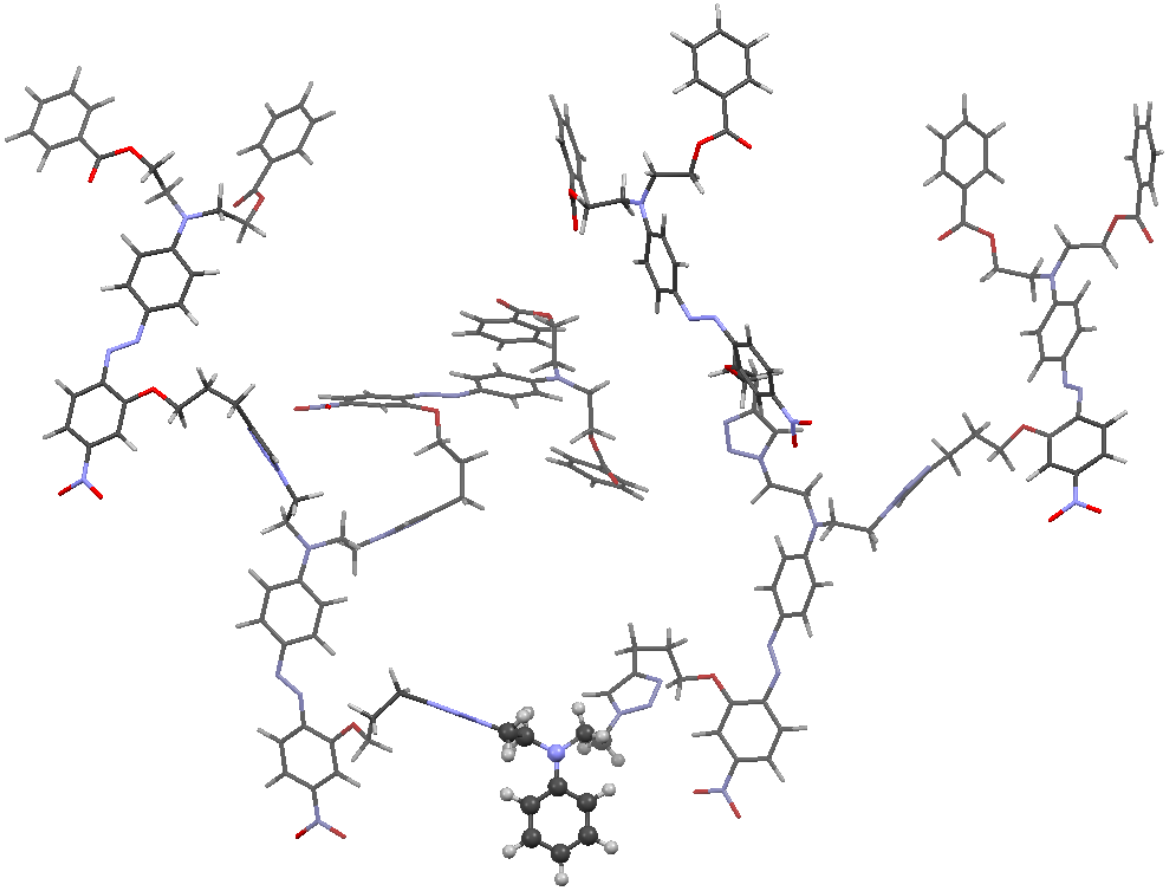

Fig. S44. The optimized structure of **G2** calculated by molecular dynamic simulation.

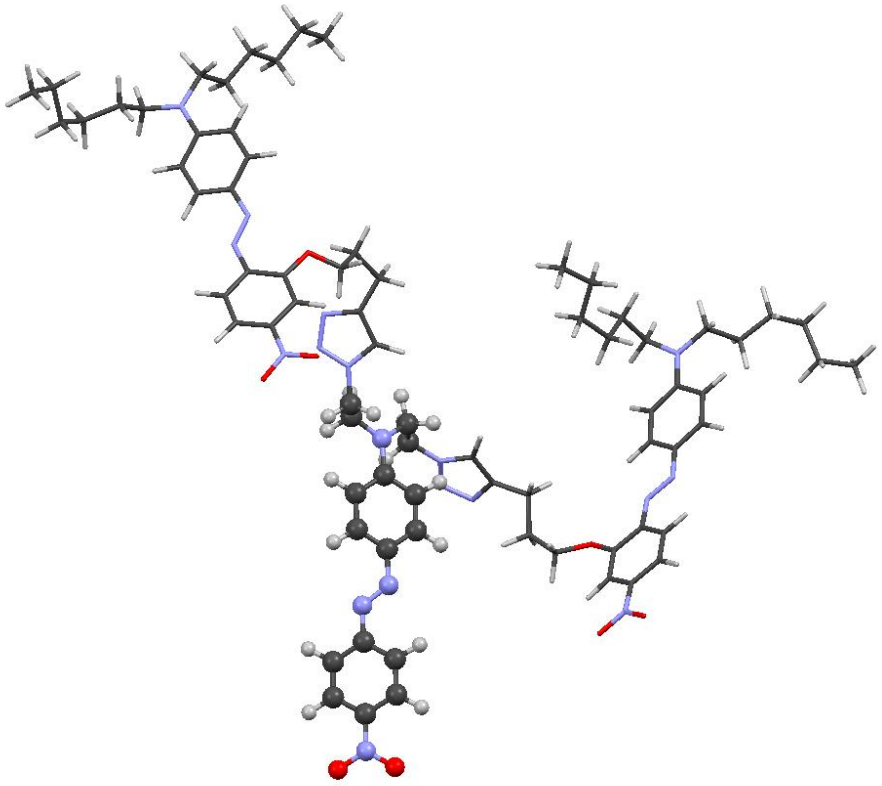

Fig. S45. The optimized structure of **C1** calculated by molecular dynamic simulation.

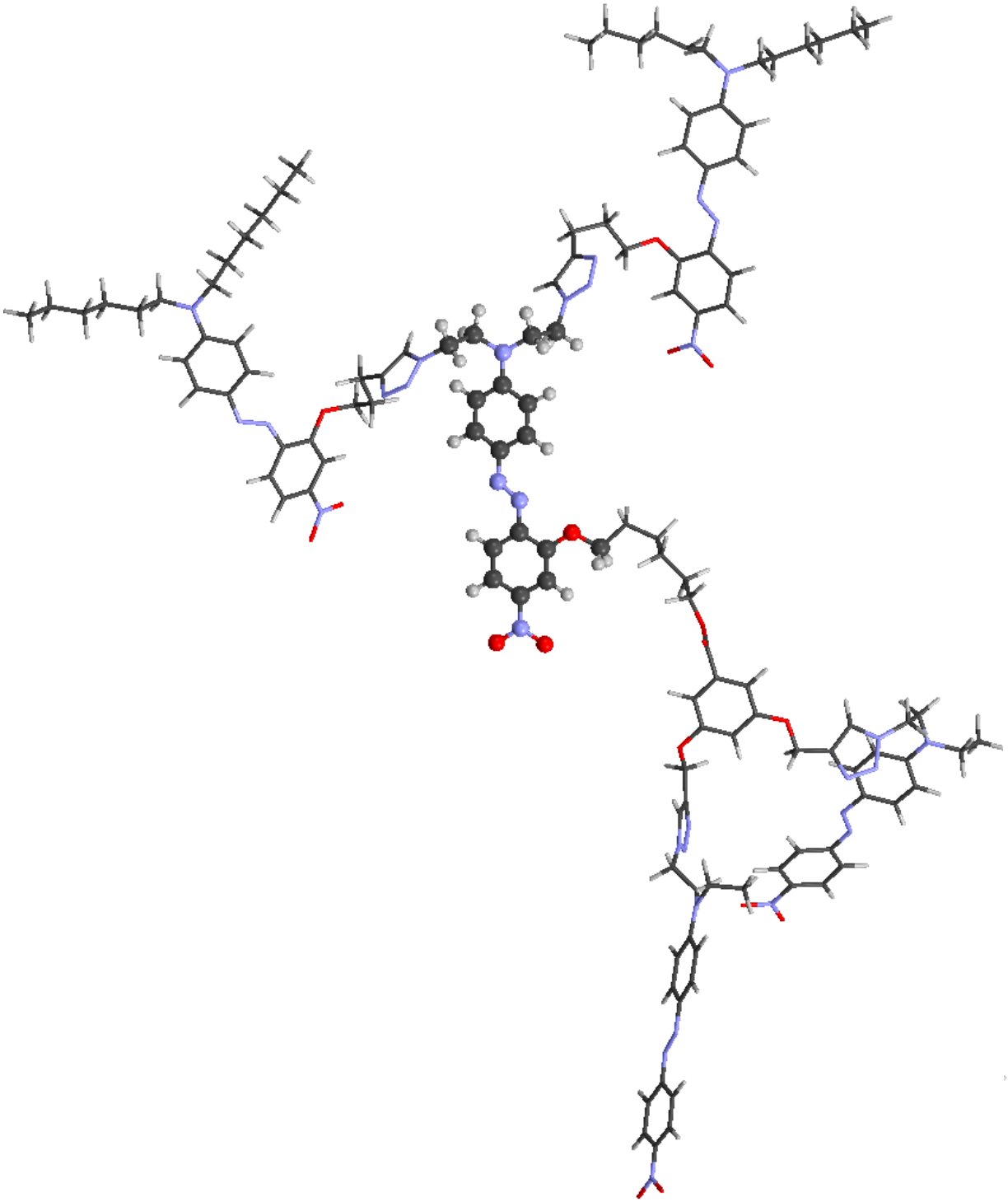

Fig. S46. The optimized structure of **C2** calculated by molecular dynamic simulation.

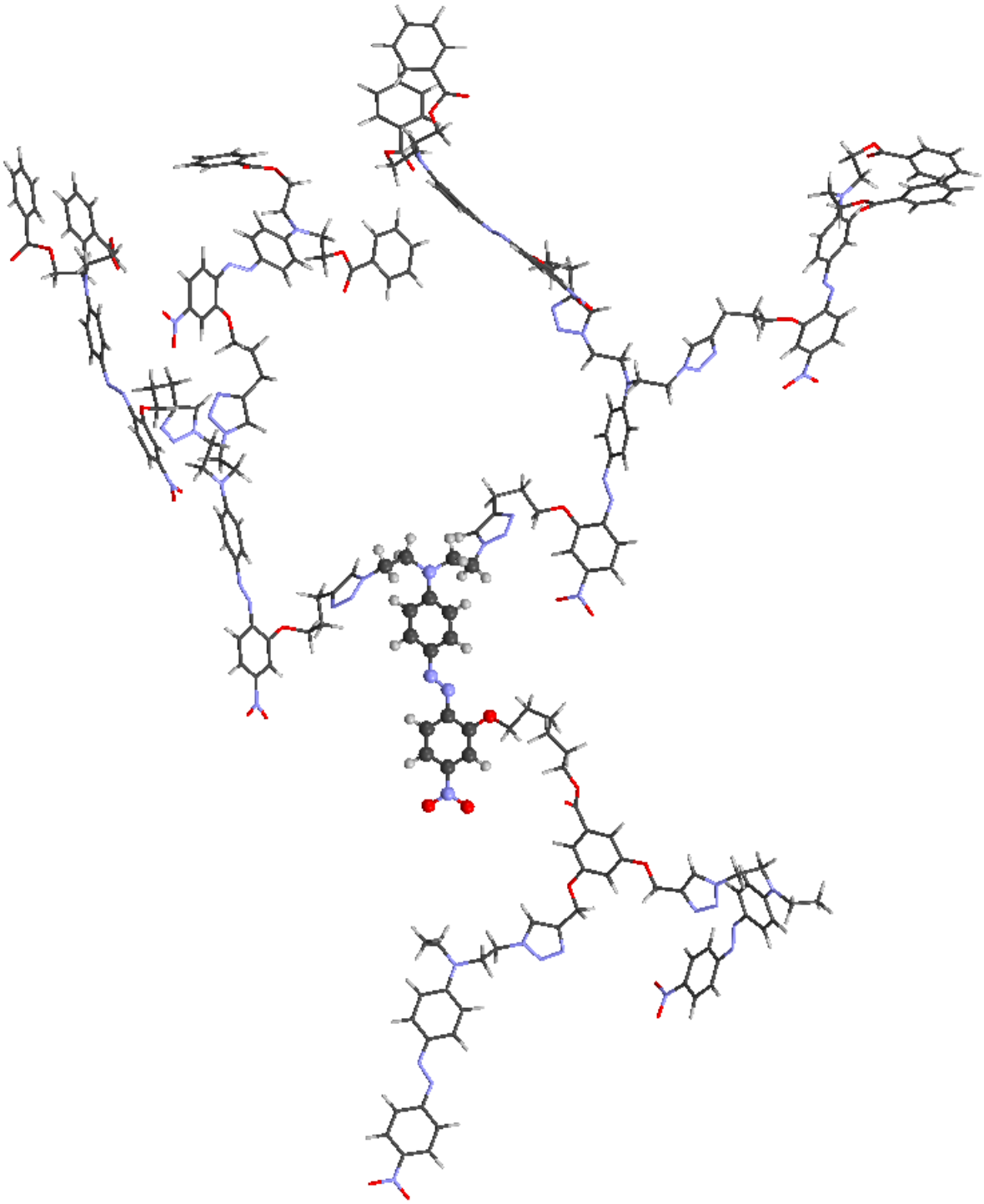

Fig. S47. The optimized structure of **C3** calculated by molecular dynamic simulation.

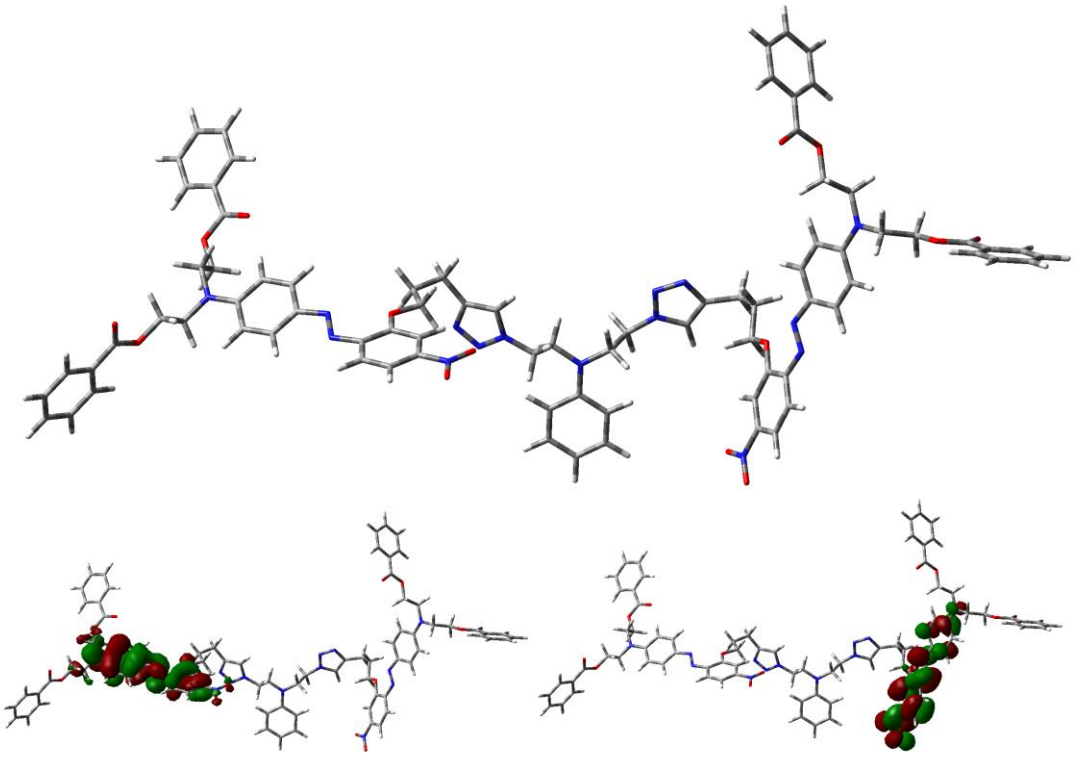

Fig. S48. The optimized structure (top) and HOMO (down left), LUMO (down right) of **G1** calculated by DFT method at B3lyp/6-31g(d).

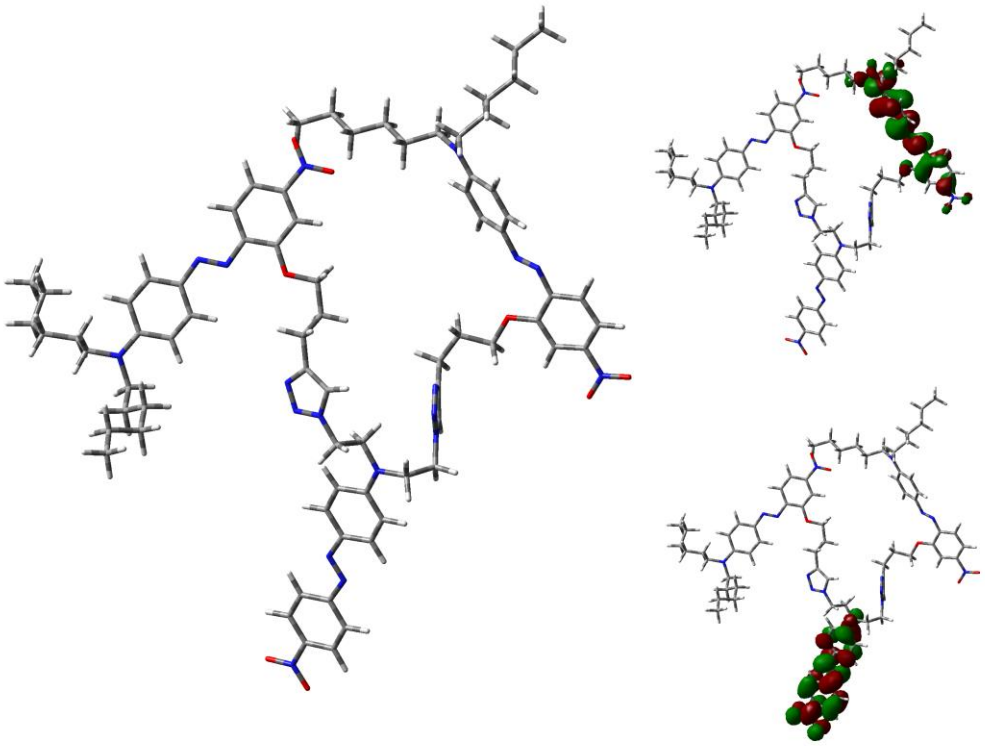

Fig. S49. The optimized structure (left) and HOMO (up right), LUMO (down right) of **C1** calculated by DFT method at B3lyp/6-31g(d).

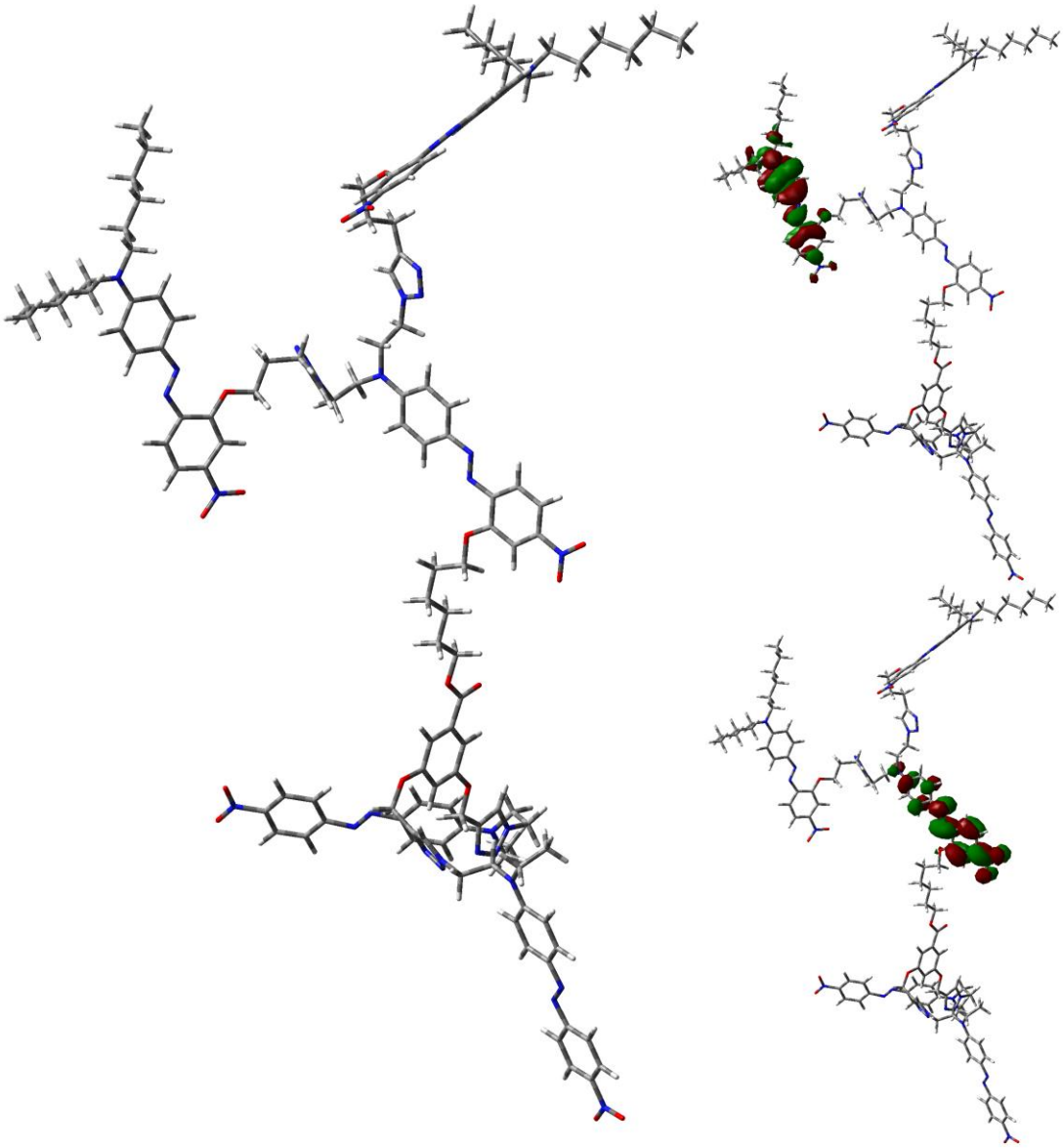

Fig. S50. The optimized structure (left) and HOMO (up right), LUMO (down right) of **C2** calculated by DFT method at B3lyp/6-31g(d).

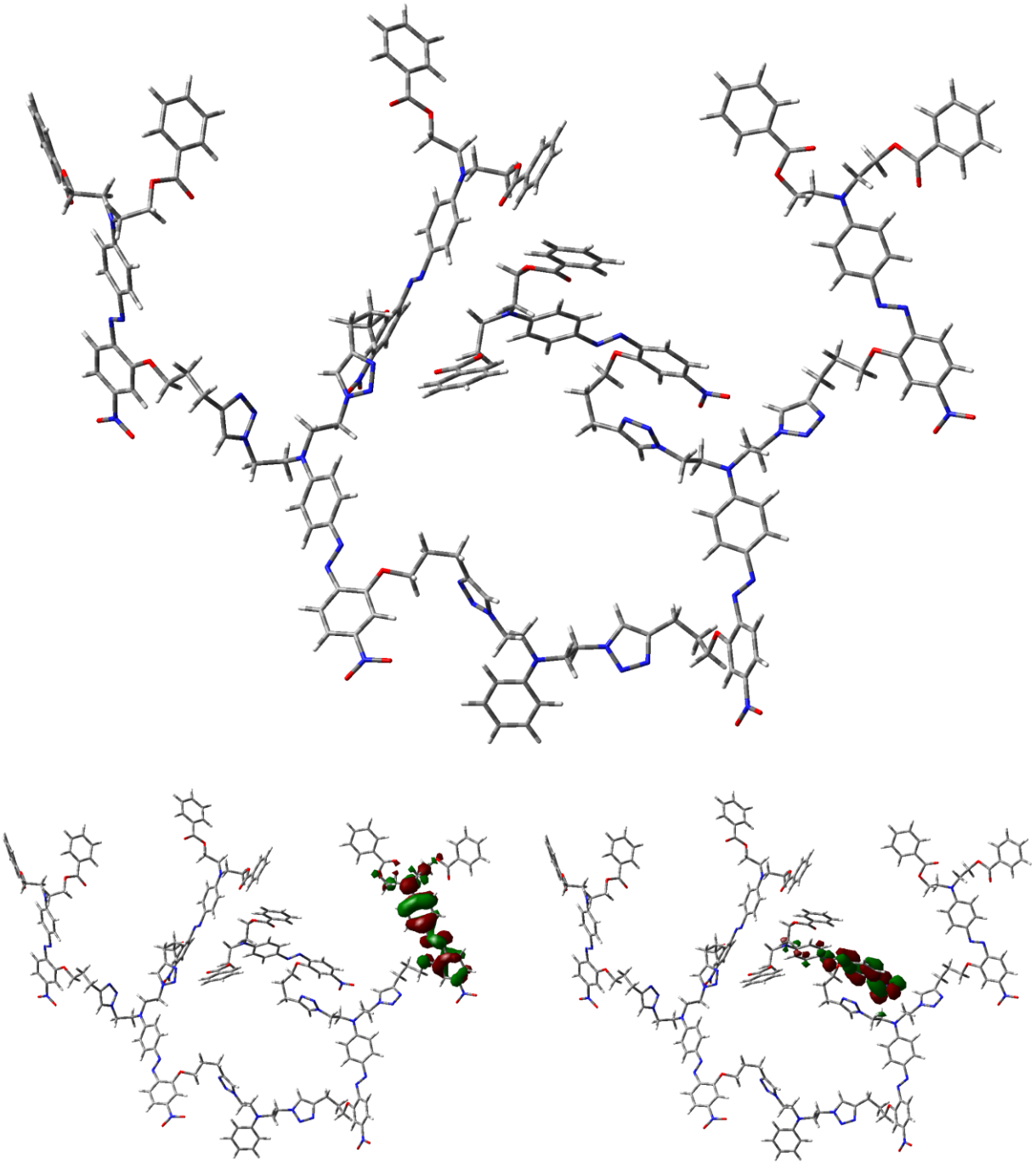

Fig. S51. The optimized structure (up) and HOMO (down left), LUMO (down right) of **G2** calculated by DFT method at B3LYP/STO-3G.

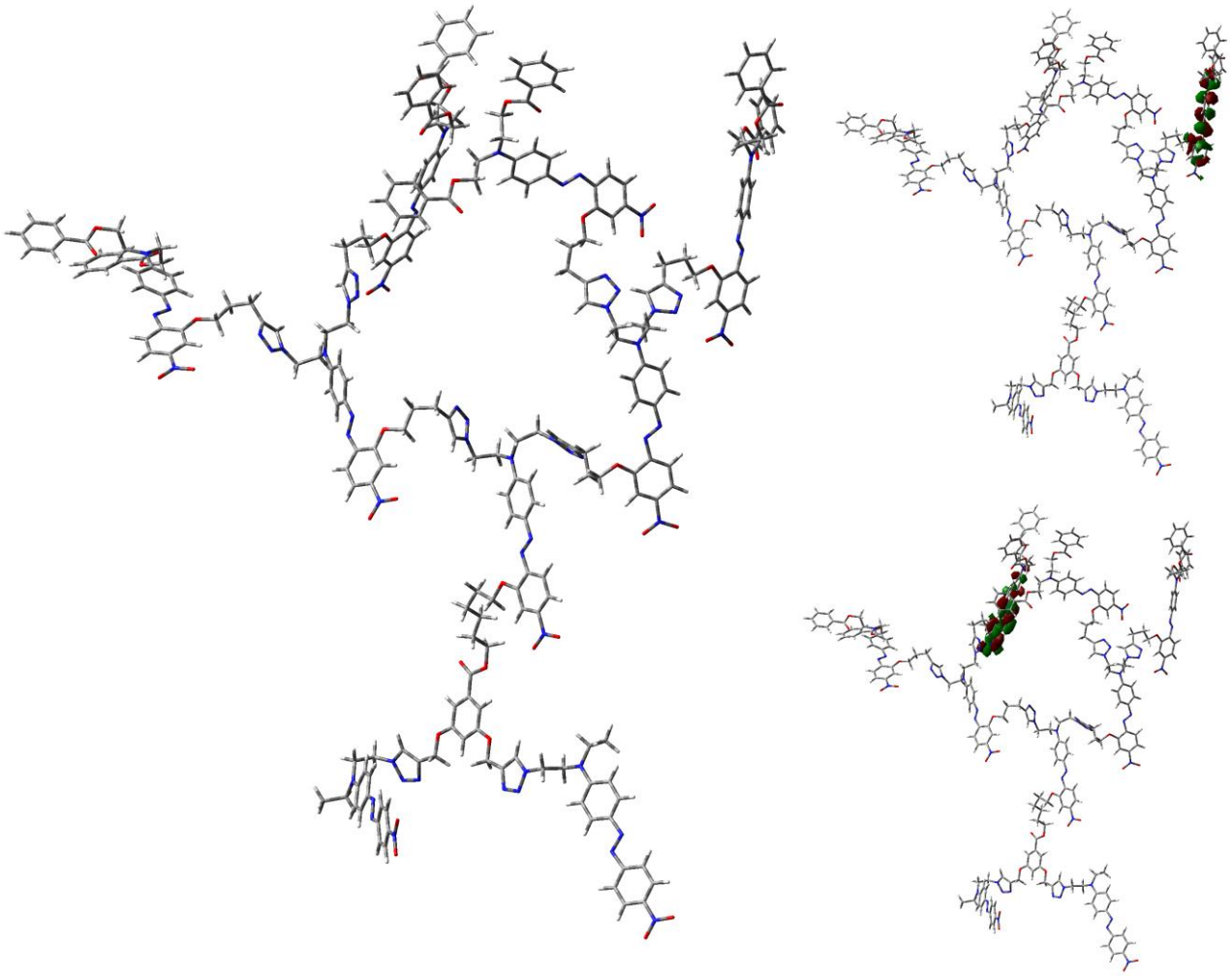

Fig. S52. The optimized structure (left) and HOMO (up right), LUMO (down right) of **C3** calculated by DFT method at B3LYP/STO-3G.

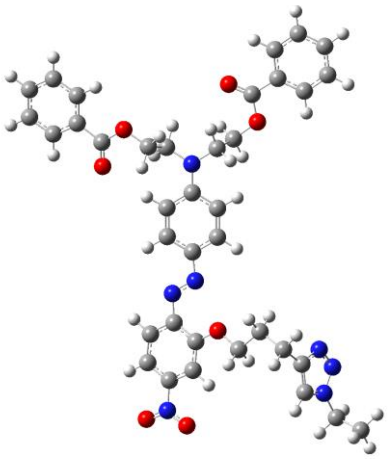

Fig. S53. The optimized structure of **Frag 1** calculated by DFT method at B3lyp/ 6-311g(d,p).

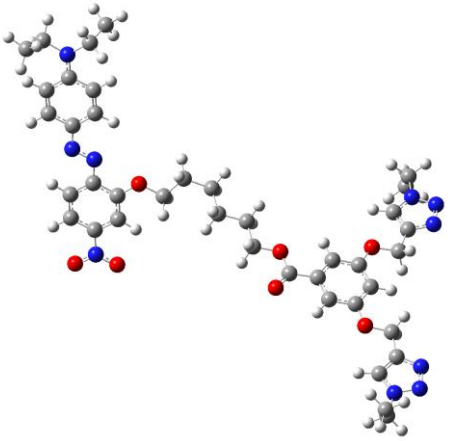

Fig. S54. The optimized structure of **Frag 2** calculated by DFT method at B3lyp/ 6-311g(d,p).

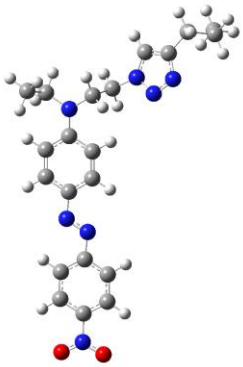

Fig. S55. The optimized structure of **Frag 3** calculated by DFT method at B3lyp/ 6-311g(d,p).